Bulletin of the Mineral Research and Exploration

http://bulletin.mta.gov.tr

Geochemistry of beach sands from the Bartın and Samsun-Ordu coastal districts, Northern Black Sea, Türkiye: implications for provenance

Pelin COŞANAY*[a] and Halim MUTLU[a]

[a] *Ankara University, Department of Geological Engineering, Ankara, Türkiye*

Research Article

Keywords:
Beach sand, Black Sea, Heavy Mineral, Mineral Chemistry, Provenance.

ABSTRACT

This study aims to investigate geochemical and petrological characteristics, chemical weathering indices and provenance of the beach sands collected from 11 different sites along the coastlines of Bartın, Samsun and Ordu districts adjacent to mafic and intermediate volcanic rocks on the Pontides. Petrological findings show that the abundance of detrital quartz, feldspar and sedimentary lithic fragments increase in beach sands of the Bartın region where the SiO_2 values fall in a wide range (47 to 87 wt.%). The Samsun and Ordu beach sands have moderately low SiO_2 (50 to 61 wt. % and 48 to 62 wt. %, respectively) and relatively high Fe_2O_3 contents. LREE concentrations of investigated beach sands show enrichment patterns. Mafic minerals, especially pyroxene and magnetite grains are represented by eroded or abraded morphologies due to dissolution and erosion processes, while opaque heavy minerals show signs of recycling from basic adjacent rocks with etched to sub-rounded grain surface textures. The low chemical index of alteration (CIA) estimated for the beach sand samples implies the presence of fresh rock erosion along the coasts. We used magnetite to gain better understanding of the formation and origin of Fe-rich beach sands. The mineral chemistry data indicate that studied magnetites have quite similar composition and the mobility of trace elements exerts a great control on their distribution in magnetite.

Received Date: 03.10.2024
Accepted Date: 07.03.2025

1. Introduction

Marine placers, which contain heavy mineral (HM) accumulations of economic importance, are formed by the changes in sea level during transgression and regression processes that occur over geological time (Force, 1991; Roy, 1999; Hou et al., 2017; Dill et al., 2018). Placers or clastic deposits originate from the accumulation of HMs, which may or may not have an economic grade, from the rocks behind the shore with different lithological characteristics. In such a process, minerals that are resistant to physical/mechanical weathering are deposited in suitable environments. HMs and HM-containing materials derived from weathered and eroded bedrock are transported by rivers to the coastal sites to accumulate along the shoreline (Force, 1976, 1991; Hou et al., 2011). The petrological, mineralogical and geochemical properties of HMs derived from the source rocks and fractionated in the coastal sands, river and dune sediments have been the subject of several studies (e.g. Hutton, 1950; Grigsby, 1990; Morton and Hallsworth, 1994; Garzanti and Ando, 2007; Yang et al., 2009; Qiu et al., 2011; Garzanti et al., 2012, 2013; Kasper-Zubillaga et al., 2016; Abdel-Karim and Barakat, 2017; Papadopoulos, 2018; Kasper-Zubillaga et al., 2021;

Citation Info: Coşanay, P., Mutlu, H. 2025. Geochemistry of beach sands from the Bartın and Samsun-Ordu coastal districts, Northern Black Sea, Türkiye: Implications for provenance.Bulletin of the Mineral Research and Exploration 177, 52-76. https://doi.org/10.19111/bulletinofmre.1653503

*Corresponding author: Pelin COŞANAY, pelincsny@gmail.com

Lohmeier et al., 2021). Coastal placer formations contain stable minerals of varying densities (e.g. magnetite, ilmenite, monazite, cassiterite, xenotime, rutile, and zircon), which are hardly altered chemically and physically (Van Gosen et al., 2014; Hou et al., 2017).

The placer deposits in Türkiye contain quite low grades of gold. However, The Manisa-Sart placer deposit in western Anatolia hosts ~73.500 oz Au. Hatay-Akıllıçay in the southern part, Manisa-Irlamaz and Sakarya-Geyve deposits in the west, and Elazığ-Harput and Bingöl-Hamek mineralizations in the eastern part are some other prospective gold placer areas in Türkiye (MTA, 1993). The Divriği iron placer, heavy mineral containing dunes around Manisa-Sart (Yiğit, 2009) and Hatay-Samandağ black beach sands (Ergin et al., 2018) are included to the placer deposits of Türkiye. The studied Holocene beach sands of the Samsun-Yeşilırmak River, Terme Stream and Ordu coasts have resources of ~10-14% Fe and 6-7% TiO_2 (Köksoy, 1973).

The aim of this study is to determine the compositional framework of beach sands in the eastern and western Black Sea coasts using the geochemical and petrological characteristics of these clastics. The study also describes the mineralogical and geochemical compositions and the provenance of terrigenous sediments of beach sands along the Black Sea coast. We characterize the beach sands using their major oxide and REE compositions and chemical index of alteration value (CIA). Finally, EPMA chemical analysis on magnetite samples provided unravelling the source of these minerals.

2. Study Area

Türkiye has the second longest coastline in the Black Sea basin following Ukraine. The study area is located at the eastern (Samsun and Ordu) and western (Bartın) parts of the Black Sea region where the North Anatolian Mountains (NAM) (so-called Pontides) extend parallel to the shoreline. The eastern part of NAM has experienced a prolonged subduction and collision and hosts active plate margins of various tectonic blocks that are closely associated with the Neo-Tethys Ocean (Kaymakcı et al., 2014). In this region, volcanic intercalated sedimentary masses of the Alpine Orogeny Belt are exposed. The Central NAM including the İstanbul and Sakarya Zones contains extensive Jurassic and Cretaceous subduction-accretion complexes (Okay et al., 2018).

The geomorphological arrangement of the Black Sea coasts, fluvial deltas and alluvial fans that are formed by varying coastal processes exerts a great control on the accumulation areas of coastal placer deposits. The geology of the Black Sea coastline differs from Bartın to Samsun and Ordu districts. The outcrops along the Bartın coast are composed of (1) Paleocene-Eocene continental clastics, (2) Jurassic clastics and carbonates, and (3) Senonian volcanics and sedimentary rocks (Figure 1a). The compositional variation of coastal sands is mainly influenced by nearby source rocks.

The rock units in the Samsun coastal region are represented by Pliocene-Pleistocene undifferentiated continental clastics and Quaternary beach and dune. Miocene basaltic rocks and Eocene volcanic and sedimentary rocks define the composition of beach sand sediment (Figure 1b). The magnetite-rich placers are widespread along the Samsun and Ordu coasts where the Upper Cretaceous andesite-pyroclastic units and Eocene volcanic and sedimentary rocks are exposed along the coastline (Figure 1b). The studied areas in Bartın are separated by a mountainous hinterland behind the narrow coastline located near the river drainage systems. In the Samsun-Ordu district, the sampled beach sites are discharged by the N-S trending major rivers and tributaries (e.g. Yeşilırmak River, Terme Stream, Miliç Stream, Cuma Stream, Ele Stream, Akçaova and Turnasuyu Streams) that run into the Black Sea. The annual rainfall over the Black Sea region averages 1000 mm with a distinct rainy season spanning from August to December.

3. Sampling and Analytical Methods

The sand samples were collected during October 2021 (Bartın coastline) (Figures 2a-2e) and September 2022 (Samsun-Ordu districts) (Figures 2f-2k). In the Samsun and Ordu regions, the samples were taken from the stream mouths that drain into the Black Sea. In the Bartın region, sampling was made from

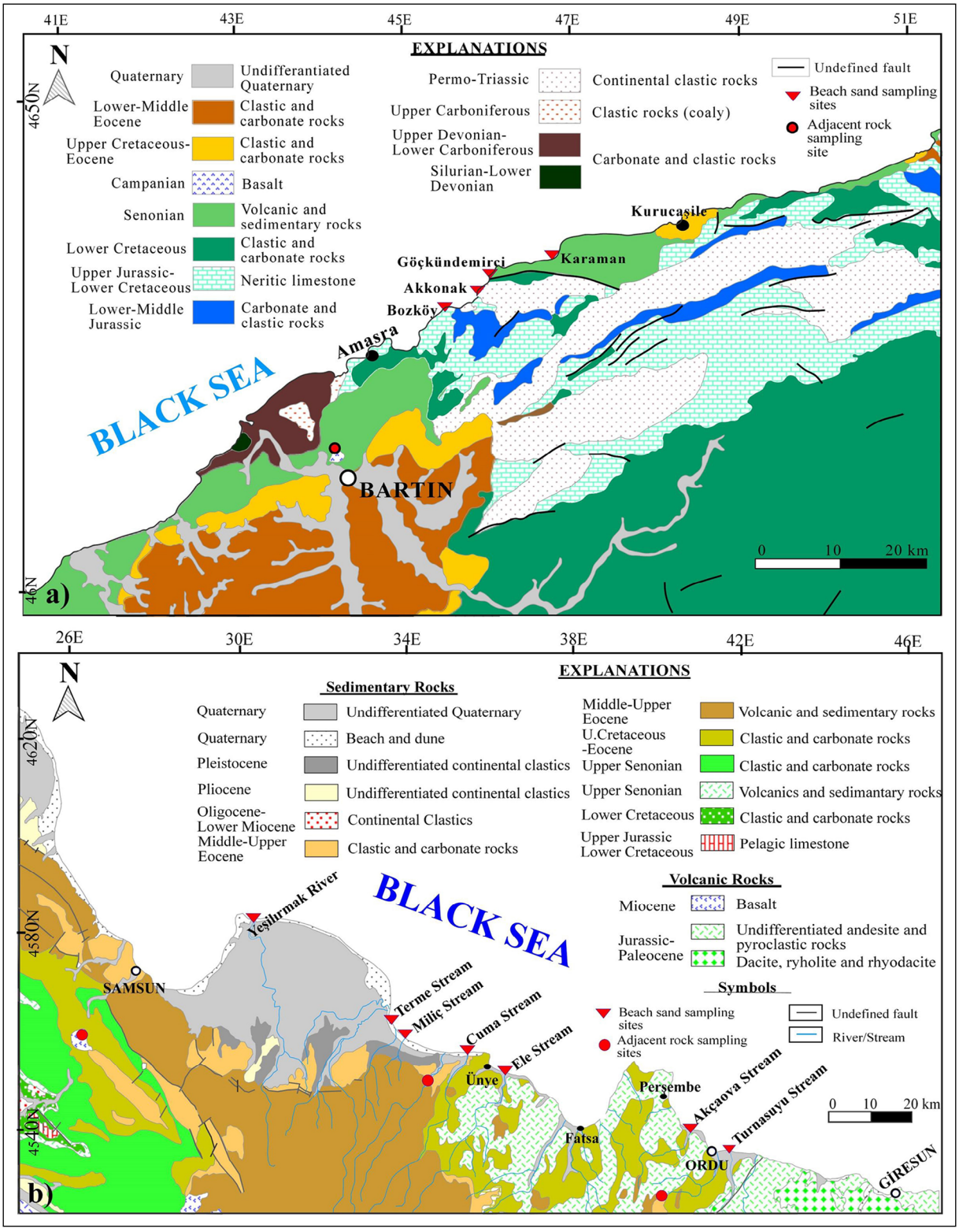

Figure 1- Simplified geological maps of study area a) Bartın (modified after (Aksay et al., 2002) and b) Samsun-Ordu (modified after (Hakyemez and Papak, 2002) districts (Beach sand and adjacent rock sampling sites indicated by red triangles with red dots, respectively).

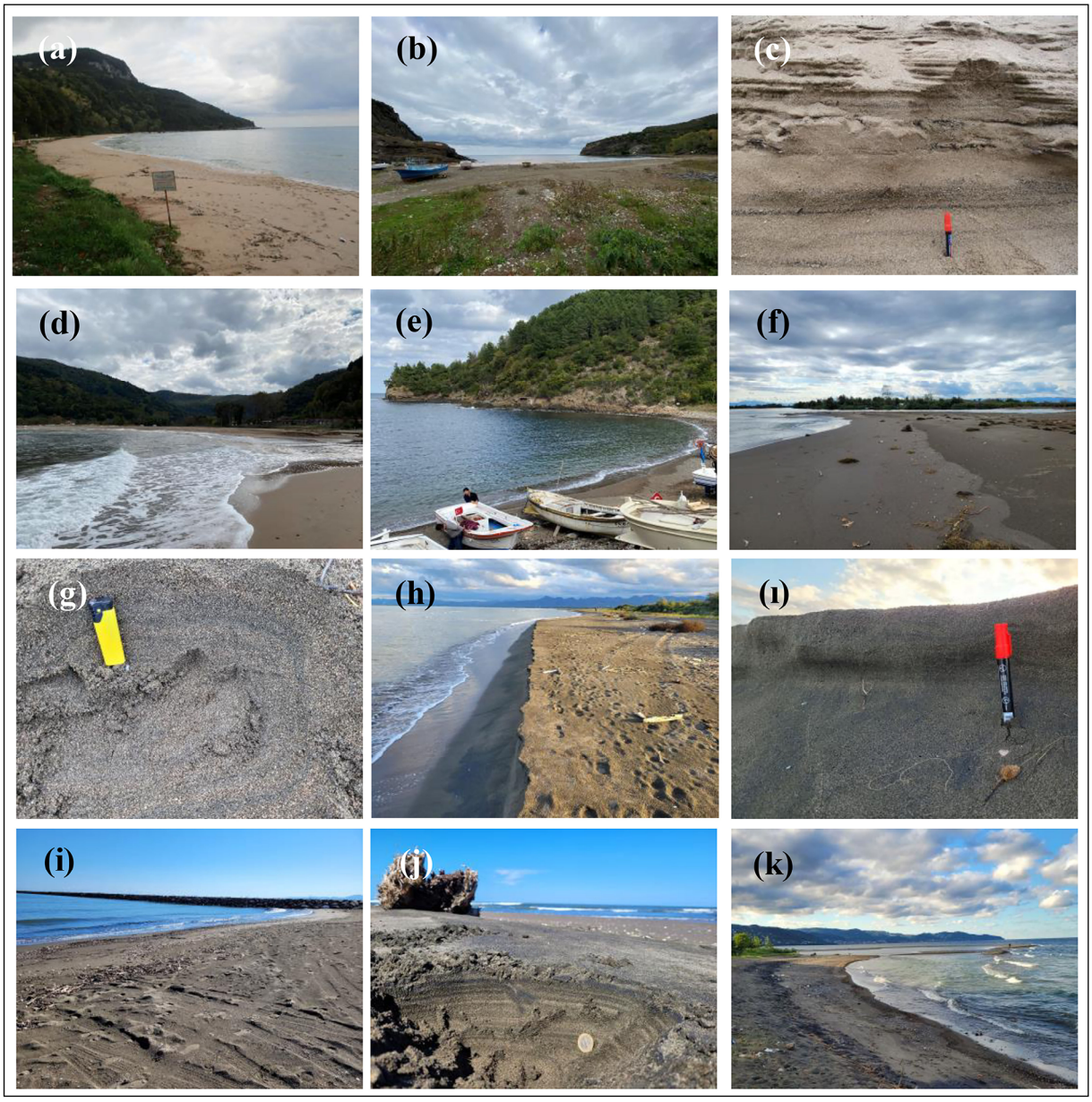

Figure 2- Sampling sites: The western Black Sea region, Bartın coastline cliffs and the width of the beach is quite narrow in the region; a) Bozköy Bay; b) Karaman Bay; c) Intermediate layers rich in dark colored heavy minerals in the Göçkündemirci beach area; d) Göçkündemirci Bay; e) Akkonak Bay coastal placer areas. Eastern Black Sea coast sampling sites: The Samsun-Ordu district investigated areas are located on beach sites where the nearly N-S trending major rivers and tributaries meets the Black Sea. Current beach sediments lie in a narrow strip at the point where tributaries drained into the Black Sea. Beach sediments consist of grayish, partly black colored laminated interlayers rich in pyroxene and opaque heavy minerls; f)-g) Samsun-Yeşilırmak, h)-ı) Samsun-Terme and i) Samsun-Miliç, j) Ünye-Cuma Stream, k) Perşembe-Akçaova.

narrow coastal beach sites. In areas where the surface is covered with organic and inorganic materials, prior to sampling, the surface was cleaned with a paddle. All the samples were collected from a depth of 5-10 cm. To investigate the relative distribution of beach sands, sampling was made proportionally to the length and width of each area. A total of 75 beach sands were sampled from eleven locations on the Bartın [Bozköy Bay (n=3); Karaman Bay (n=8); Göçkündemirci Bay (n=13) and Akkonak Bay (n=3)], Samsun [Yeşilırmak River (n=10); Terme Stream (n=5); Miliç Stream (n=8)] and Ordu [Cuma Stream (n=9); Ele Stream (n=4); Akçaova Stream (n=8); Turnasuyu Stream (n=4)] coastal sites. In addition,

4 adjacent volcanic rocks were collected close to the river/stream drainage areas that are considered as the possible magnetite bearing host rocks.

To investigate petrographic and mineralogical characteristics, each bulk sand sample was impregnated with araldite and cut into a standard petrographic thin section and examined by a polarizing microscope. Undefined detrital grains were characterized by Raman spectroscopy at the Earth Science Applications and Research Center (YEBİM), Ankara University.

Sand samples and host rocks were analyzed for the major oxide contents. For XRF analyses, samples were ground in an agate mortar and mixed with 4 g powdered sample and 0.9 g binder (wachs), compressed for the form of press-lozenge under an automatic hydraulic press (La Tour, 1989). The major oxide composition of bulk sand samples was determined from powder pellets by the Polarized Energy Dispersive (PED) XRF technique with Spectro XLab Pro instrument at the YEBİM. The spectrometer operated under a vacuum system. XRF measurements were performed with the spectrometer detector under a vacuum system equipped with a Rh anode X-ray tube and a 5-mm Be side window, which operates with <150eV resolution on Mn Kα, Si (Li) and cooled with liquid N_2 at 5000 cps (Stephens and Calder, 2004; Kadıoğlu et al., 2022). Samples were prepared for distinctive USGS standards and analyzed for rocks and mineral standard samples. The detection limit is 0.01% for major oxides. Analytical errors do not exceed 0.78% for major oxides (Na_2O: 0.34-0%; MgO: 0.09-0.03%; Al_2O_3: 0.09-0%; SiO_2: 0.13-0.08%; P_2O_5: 0.01-0.0006%; K_2O: 0.026-0.0069%; CaO: 0.04-0.009%; TiO_2: 0.009-0.0013%; V_2O_5: 0.0037-0%; Cr_2O_3: 0.0046-0%; MnO: 0.0031-0.00071%; Fe_2O_3: 0.02-0.0021%).

REE analysis of sand samples and host rocks was carried out at SGS Mining and Geochemistry Laboratory by ICP-MS and ICP-AES methods with detection limits ranging from 0.01 to 0.05 ppm. Following the sample preparation stage consisting of crushing and pulverization processes, 0.5 g sample was subjected to multi-acid digestion, which is based on acid dissolution and fuming with a combination of HNO_3 (nitric acid), HF (hydrofluoric acid), $HClO_4$ (perchloric acid) and HCl (hydrochloric acid). This is a very effective dissolution procedure for a large number of mineral types and is suitable for a wide range of elements. Trace element concentrations were analyzed with a PerkinElmer NexION 1100 ICP mass spectrometer with a single gas channel. Detection limits range from 0.01 to 0.05 ppm. The analysis uses test methods of ASTM E1479 and E2371.

The chemical composition of magnetite grains was determined only for the Samsun and Ordu samples. For this, sixteen polished and carbon-coated thin sections were analyzed by JEOL JXA-8230-EPMA at the YEBİM, Ankara University. Before the analysis, detrital magnetite grains were collected by a magnet bar. In each thin section, 3 to 8 magnetite grains were analyzed for major oxides and trace elements under an accelerating voltage of 20 kV, 10 nA beam current, and beam diameter of 1 µm. Electron microprobe is equipped with both wave (WDS) and energy dispersive (EDS) spectrometers. Trace element analyses were carried out with long count-times (up to 200 sec). Natural oxide standards and mineral reference materials used for calibration and measurements are; diopside (Mg, Ca), olivine (Si), rhodonite (Mn), albite (Al), iron oxide (Fe), Calc-std (Ni, Ga, Ge, Sn, Sc, Pb, W, Mo), Co -std (Co), Cu-std (Cu), titanium oxide (Ti), chromium oxide (Cr), Nb-std (Nb), apatite (P), tantalum (Ta), zircon oxide (Zr), Hf-std (Hf) and zinc (Zn). The standard limits for each element are Mg (150 ppm), Si (196 ppm), Mn (94 ppm), Al (89 ppm), Co (1662 ppm), Cu (831 ppm), Fe (364 ppm), Ti (69 ppm), Cr (48 ppm), V (91 ppm), Nb (239 ppm), P (89 ppm), Pb (337 ppm), Ta (459 ppm), Zr (244 ppm), Ca (39 ppm), Hf (188 ppm), Y (284 ppm) and Zn (139 ppm). Matrix and atomic number (Z) effects, absorbance (A) and fluorescence (F) were corrected using ZAF software provided by JEOL.

4. Results

4.1. Petrographical Framework

4.1.1. Bartın Province

The detrital minerals in sand-size sediments sampled from different coastal areas in the Bartın region are composed predominantly of quartz, K-feldspar, carbonates, plagioclase and dominantly of

altered opaque heavy minerals and pyroxene derived from volcanic rocks of microlithic texture. Mafic minerals and lithic grains altered to Fe-oxides (Figures 3a and 3b) and limonite. Lithic grains are mainly of sedimentary and altered volcanic clastics distributed within a microlitic mass (Figure 3b). Silicification and rare epidotisation are present in detrital andesitic basalt rock fragments. Some proportions of minerals and lithic fragments show angled to rounded morphology with etched and rough surface. In the Bartın province, beach sands do not contain detrital opaque heavy minerals. Plagioclase phenocrysts and amphibole in fine-grained groundmass were observed in adjacent basalt and/or andesitic basalt source rock (Figure 3d).

4.1.2. Samsun and Ordu Provinces

Beach sand samples collected from the Samsun region consist mainly of pyroxene, plagioclase, carbonate, and opaque heavy minerals (magnetite and hematite). Kelyphitic rims are common around the pyroxene grains (Figures 4a and 4b). Magnetite occurs within lithic fragments (Figure 4c), or it forms individual grains (Figures 4b and 4d). The rock fragments identified under the microscope are lithic volcanic grains (Lv) with microlithic texture (Figures 4c and 4d) and basic lithic fragments of gabbroic adjacent rock, mainly rich in plagioclase, pyroxene and amphibole crystals with granular-porphyritic textures (Figure 5a).

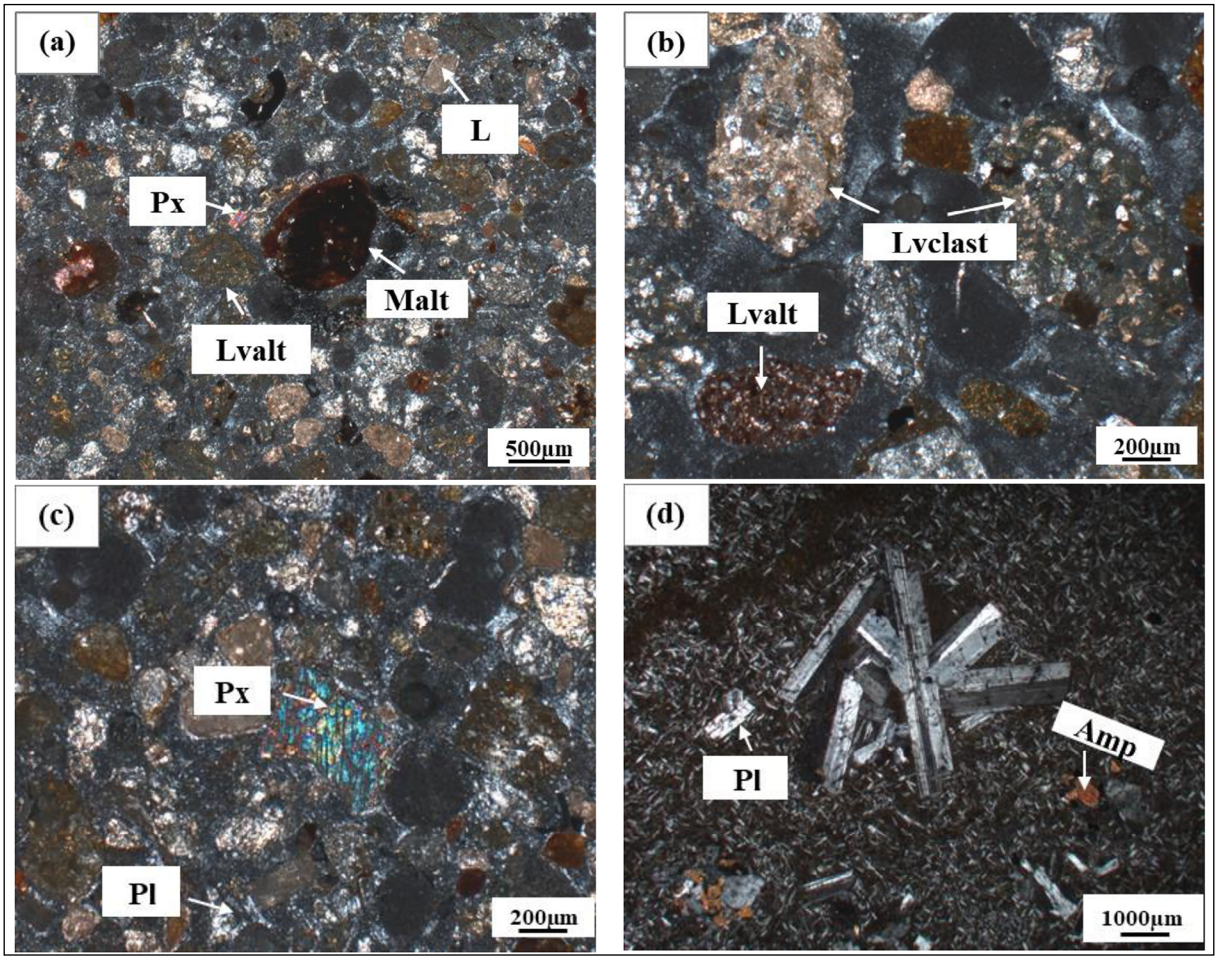

Figure 3- Photomicrographs of thin sections. Detrital grains within bulk sand samples and adjacent rock from the Bartın district illustrate distinctive mineralogical and textural features. a) Bartın-Karaman; altered/oxidized mafic mineral (Malt) and lithic fragment (Lvalt), b) Bartın-Akkonak: Altered lithic volcanic fragments (Lvalt) with microlitic texture and brown glassy groundmass and lithic volcaniclastic grains. c): Bartın-Karaman; detrital pyroxene and plagioclase grains. d) Bartın-Basalt sample with euhedral plagioclase and fine brown amphibole phenocrysts in fine-grained/glassy groundmass. *(Lvalt: Altered lithic volcanic; Lvclast: Lithic volcaniclastic; Malt: Altered mafic mineral; Mag: Magnetite; Px: Pyroxene; Pl: Plagioclase; L: Limestone; Amp: Amphibole).*

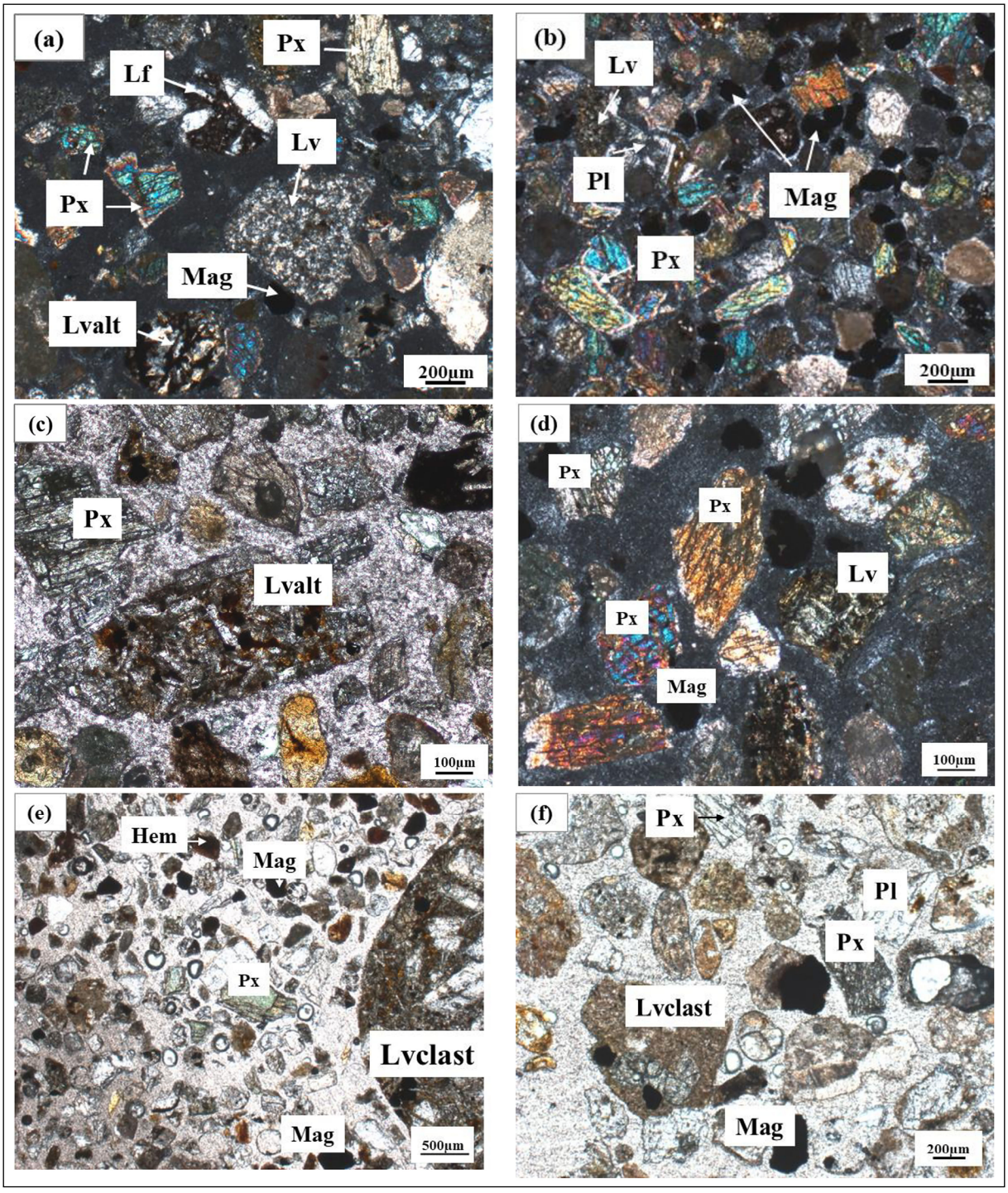

Figure 4- Photomicrographs of petrographic thin sections of bulk sand samples from the Samsun and Ordu districts. a) Samsun-Yeşilırmak; altered felsic lithic grain (Lf), opaque minerals within a microlitic volcanic lithic fragment (Lv) and altered volcanic lithic grain (Lvalt), pyroxene and magnetite. b) Samsun-Terme; volcanic lithic grain (Lv), magnetite, pyroxene and plagioclase. c) Samsun-Miliç: Altered volcanic lithic grain (Lvalt) with microlitic texture and pyroxene. d) Lithic volcanic grain (Lv), pyroxene and magnetite. e-f) Ordu-Cuma Stream; volcaniclastic lithic fragment (Lvclast), pyroxene, hematite, magnetite and plagioclase. *(Lf: Felsic lithic; Lv: Volcanic lithic; Lvclast: Lithic volcaniclastic; Mag: Magnetite; Hem: Hematite; Px: Pyroxene; Pl: Plagioclase).*

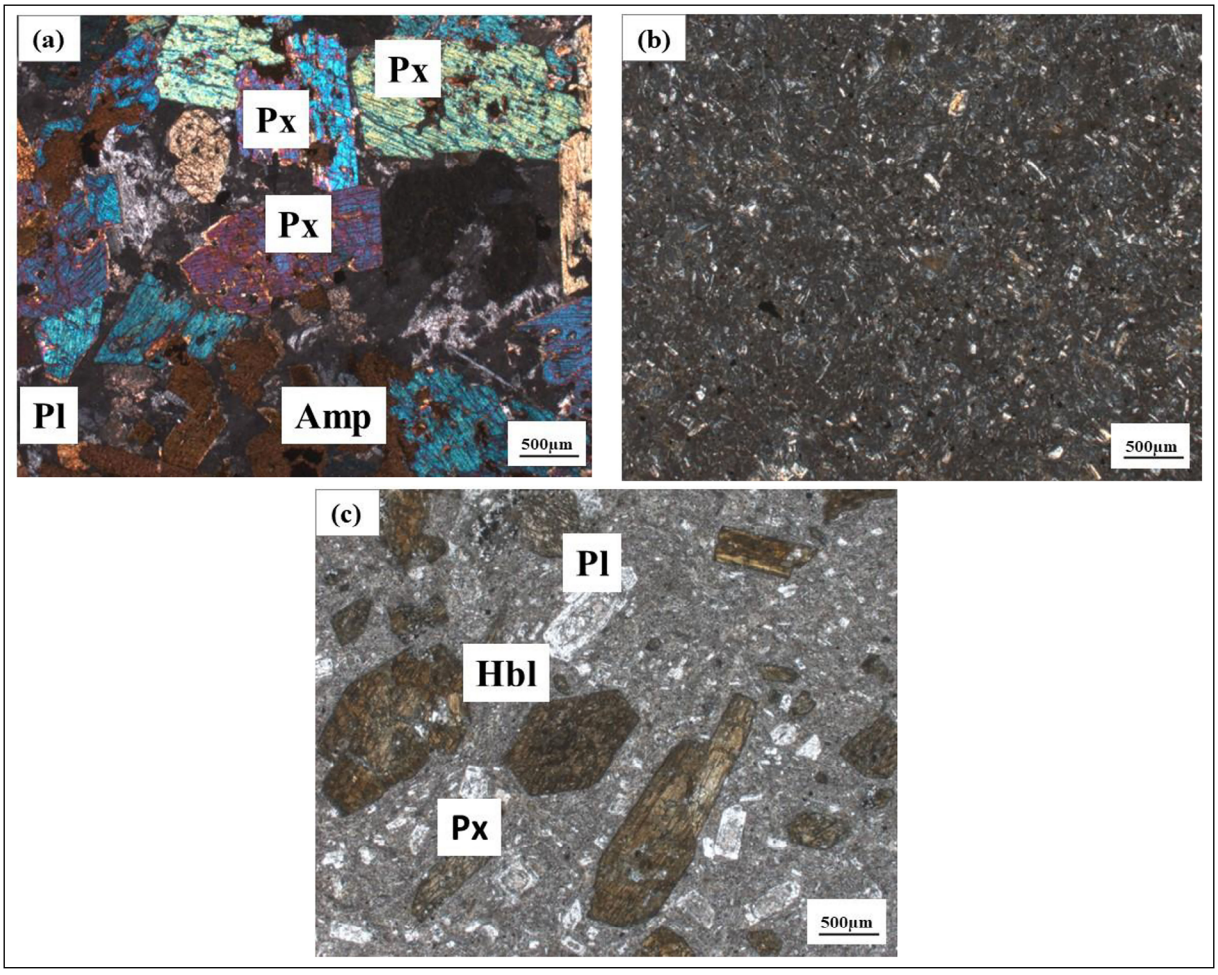

Figure 5- Photomicrographs of petrographic thin sections of adjacent host rocks from the Samsun and Ordu districts, a) Samsun-Gabbro: Clinopyroxene and plagioclase crystals in cumulate textured gabbro showing opaque Fe-oxide grains in pyroxene, disseminated and within interstitial spaces between pyroxene, b) Ordu-Basalt: Plagioclase microlites and pyroxene minerals in the glassy groundmass, c) Ordu-Andesite: Zoned plagioclase and hornblend crystal in andesitic rock. (*Px: Pyroxene; Pl: Plagioclase; Hbl: Hornblende; Amp: Amphibole).*

The sand samples from the Ordu region are composed of rock fragments, pyroxene, plagioclase, opaque heavy minerals (magnetite and hematite) and biosparitic limestone grains. The rock fragments are made up of plagioclase-rich lithic volcanic grains within a microlithic texture (basaltic and/or andesitic origin) and volcaniclastic lithic fragments (Lvclast) (Figures 4e and 4f).

The abundance of volcanic rock fragments, volcaniclastic lithics and some limestone grains in the Samsun and Ordu beach sands reveal the relative abundance of a heterogeneous adjacent source rock composed of volcanic origin (Figures 5a-5b and 5c).

4.2. Bulk Beach Sand Major Element Geochemistry

Results of major oxide analyses (wt%) (Table 1, Table 2 and Table 3) show that Bartın beach sands are represented by quite high SiO_2 concentrations (average 72%) and low Al_2O_3, Fe_2O_3 and TiO_2 contents (with averages of 6.14%, 4.29% and 0.26%, respectively). However, Bartın-Bozköy and Göçkündemirci beach sand samples indicate lower Na_2O content compared to the other sites (Karaman and Akkonak Bays). Average Fe_2O_3 contents are quite high in Bartın-Karaman and Akkonak Bay (with ave 8.15% and 8.92%, respectively) probably indicating that the sediments were derived from Fe-rich basaltic

Table 1- Major (wt%) element data of the Bartın beach sands and adjacent rock.

Sampling site	Sample type and no	Easting 455863	Northing 4624916													
Bartın-Bozköy Bay (n=3)	Beach sand sample no	SiO_2	Al_2O_3	Fe_2O_3	MgO	CaO	Na_2O	K_2O	TiO_2	P_2O_5	MnO	V_2O_5	Cr_2O_3	LOI	Sum	CIA
	BRT-01	69.92	0.04	0.01	0.27	0.01	2.08	14.74	0.04	0.42	0.01	0.00	0.00	11.92	99.46	0.03
	BRT-02	77.08	0.04	0.01	0.25	0.02	1.04	8.46	0.04	0.42	0.01	0.00	0.00	12.92	100.29	0.05
	BRT-03	77.89	0.03	0.01	0.43	0.01	1.35	8.74	0.04	0.41	0.01	0.00	0.08	10.91	99.91	0.05
Bartın-Karaman Bay (n=8)		Easting 468418	Northing 4630795													
	BRT-04	66.69	0.33	7.17	11.85	0.09	1.95	5.92	1.29	1.54	0.06	0.02	0.00	3.77	100.67	33.02
	BRT-05	63.90	0.51	11.20	5.94	0.13	2.44	6.38	1.64	1.99	0.08	0.03	0.00	5.93	100.16	40.52
	BRT-06	68.76	0.40	9.44	4.64	0.10	2.12	5.24	1.12	1.75	0.06	0.02	0.01	6.85	100.52	41.60
	BRT-07	58.13	0.53	16.37	9.62	0.12	3.50	6.46	2.44	2.01	0.03	0.02	0.00	0.68	99.91	47.70
	BRT-08	56.08	0.47	15.35	5.47	0.11	2.37	5.30	1.25	1.78	0.08	0.03	0.00	11.84	100.14	52.98
	BRT-09	47.65	0.61	13.33	10.25	0.15	2.88	4.83	1.32	2.01	0.15	0.03	0.00	16.88	100.09	50.38
	BRT-10	49.26	0.54	15.27	12.59	0.13	2.59	5.10	0.84	1.88	0.07	0.03	0.00	11.91	100.21	54.63
	BRT-11	49.14	0.40	14.50	4.84	0.10	5.63	9.57	0.92	1.46	0.60	0.05	0.22	12.85	100.30	41.43
Bartın-Göçkündemirci Bay (n=13)		Easting 462159	Northing 4628327													
	BRT-22	78.34	0.14	2.97	1.33	0.05	0.81	2.35	1.10	1.02	0.02	0.00	0.03	11.79	99.93	29.24
	BRT-23	81.81	0.11	2.04	3.09	0.04	0.74	2.25	0.74	0.91	0.13	0.01	0.02	8.99	100.88	24.50
	BRT-24	83.13	0.11	2.22	0.96	0.04	0.63	1.84	0.53	1.08	0.02	0.01	0.00	9.78	100.33	29.21
	BRT-25	80.18	0.18	2.80	1.84	0.08	0.93	4.28	1.08	0.79	1.51	0.02	0.05	6.90	100.62	21.16
	BRT-26A	85.24	0.11	1.72	1.05	0.03	0.69	1.61	0.73	1.00	0.03	0.01	0.07	7.69	99.96	24.85
	BRT-26B	79.84	0.16	2.92	1.56	0.09	0.95	4.45	0.84	0.89	0.03	0.01	0.01	9.04	100.79	21.89
	BRT-26C	83.69	0.13	1.99	1.41	0.05	0.82	3.09	0.83	0.77	0.03	0.01	0.05	7.95	100.82	20.26
	BRT-27	85.07	0.08	1.75	0.74	0.02	0.55	1.15	0.76	1.05	0.01	0.00	0.03	9.38	100.59	28.10
	BRT-28	81.69	0.12	1.98	1.47	0.04	0.71	2.46	1.06	0.91	0.97	0.04	0.27	9.12	100.85	21.54
	BRT-29	84.91	0.16	1.88	1.35	0.05	0.76	2.34	0.52	0.90	0.03	0.01	0.04	7.78	100.73	23.56
	BRT-30	85.93	0.15	1.59	1.42	0.04	0.80	2.30	0.90	0.86	0.02	0.01	0.05	5.98	100.05	19.38
	BRT-31	83.33	0.14	2.18	1.38	0.05	0.71	2.08	0.82	0.92	0.02	0.01	0.08	8.83	100.54	26.23
	BRT-37	87.62	0.10	1.31	1.00	0.04	0.67	1.99	0.37	0.83	0.02	0.01	0.03	5.94	99.92	20.39
Bartın-Akkonak Bay (n=3)		Easting 458790	Northing 4627530													
	Beach sand sample no	SiO_2	Al_2O_3	Fe_2O_3	MgO	CaO	Na_2O	K_2O	TiO_2	P_2O_5	MnO	V_2O_5	Cr_2O_3	LOI	Sum	CIA
	BRT-38	67.73	0.45	7.01	5.35	0.08	2.55	7.97	2.39	0.85	0.07	0.03	0.02	5.95	100.44	26.61
	BRT-39	55.23	0.36	12.23	9.93	0.06	1.96	9.32	2.34	1.07	0.11	0.02	0.01	7.92	100.56	35.77
	BRT-40	56.88	0.36	12.47	11.48	0.07	2.77	9.41	2.48	0.88	0.07	0.02	0.05	2.91	99.86	36.03
		Easting 446206	Northing 4612060													
Adjacent rock	Bartın-Basalt	63.55	15.39	4.93	1.21	1.55	4.96	6.25	0.75	0.28	0.12	0.02	0.00	0.73	99.01	

Table 2- Major (wt%) element data of the Samsun beach sands and adjacent rock.

Sampling site	**Sample type and no**	**Easting** 304322	**Northing** 4583599													
Samsun-Yeşilırmak River (n=10)	**Beach sand sample no**	**SiO_2**	**Al_2O_3**	**Fe_2O_3**	**MgO**	**CaO**	**Na_2O**	**K_2O**	**TiO_2**	**P_2O_5**	**MnO**	**V_2O_5**	**Cr_2O_3**	**LOI**	**Sum**	**CIA**
	SY-01	51.74	10.05	9.24	5.63	11.92	1.24	1.62	0.67	0.17	0.13	0.03	0.11	7.75	100.28	28.62
	SY-02	54.58	9.13	7.51	4.94	11.26	1.24	1.56	0.70	0.15	0.12	0.04	0.10	8.04	99.36	27.70
	SY-03	55.19	8.29	9.65	5.04	11.73	0.69	1.30	0.58	0.16	0.12	0.03	0.07	7.09	99.95	26.07
	SY-04	56.99	9.01	6.83	5.09	11.76	0.80	1.44	0.64	0.15	0.12	0.03	0.14	6.98	99.98	27.38
	SY-05	56.93	8.37	8.02	5.92	12.75	0.83	1.24	0.72	0.14	0.14	0.03	0.12	3.93	99.14	24.67
	SY-06	50.04	8.70	16.66	4.63	11.25	1.06	1.45	0.59	0.16	0.12	0.03	0.06	5.95	100.70	27.12
	SY-07	57.70	9.08	6.35	4.71	10.83	0.96	1.63	0.57	0.16	0.14	0.03	0.09	7.05	99.29	28.62
	SY-08	57.41	9.25	5.91	4.67	9.90	1.55	1.71	0.53	0.16	0.10	0.03	0.06	8.84	100.10	29.57
	SY-09	53.17	8.44	9.95	4.95	11.23	0.98	1.44	0.63	0.13	0.12	0.03	0.09	8.78	99.95	26.63
	SY-10	52.85	8.58	9.69	4.93	11.84	1.05	1.46	0.51	0.13	0.11	0.02	0.04	9.05	100.27	25.91
Samsun-Terme Stream (n=5)		**Easting** 334653	**Northing** 4564230													
	ST-01	54.35	6.33	11.29	5.97	14.60	0.06	0.79	1.12	0.13	0.18	0.06	0.31	4.29	99.48	18.90
	ST-02	52.62	7.49	12.84	7.37	15.48	0.10	0.88	1.36	0.14	0.21	0.07	0.44	0.86	99.86	20.57
	ST-03	58.00	9.01	7.70	5.33	11.89	1.30	1.51	0.75	0.16	0.14	0.04	0.15	3.32	99.30	26.49
	ST-04	55.12	9.07	7.52	5.02	11.15	0.97	1.66	0.51	0.13	0.11	0.03	0.04	8.82	100.14	27.99
	ST-05	57.07	8.57	7.43	4.71	11.66	1.48	1.57	0.51	0.13	0.11	0.02	0.04	6.85	100.15	25.50
Samsun-Miliç Stream (n=8)		**Easting** 335096	**Northing** 4561333													
	SM-01	59.69	10.32	9.22	3.39	6.06	1.44	2.15	0.42	0.15	0.10	0.01	0.02	7.83	100.80	40.21
	SM-02	59.04	10.49	6.87	4.83	9.81	1.44	1.79	0.62	0.15	0.14	0.03	0.05	4.42	99.68	32.50
	SM-03	56.72	9.51	10.07	4.53	9.32	1.22	1.76	0.54	0.15	0.12	0.03	0.04	7.01	101.02	31.67
	SM-04	60.63	10.51	8.61	4.45	8.03	1.47	1.96	0.46	0.15	0.11	0.02	0.04	3.92	100.36	35.88
	SM-05	54.81	12.26	16.35	4.68	5.58	1.54	2.21	0.48	0.14	0.11	0.02	0.01	1.65	99.83	45.42
	SM-06	57.92	10.82	8.17	4.48	8.40	1.40	2.02	0.51	0.16	0.13	0.02	0.03	6.83	100.89	35.83
	SM-07	56.50	10.65	8.00	5.12	10.45	1.48	1.79	0.55	0.15	0.13	0.02	0.05	4.97	99.85	31.63
	SM-08	61.87	10. 84	4.88	4.92	9.04	1.76	1.95	0.48	0.16	0.11	0.02	0.07	3.98	100.09	33.97
Adjacent rock	Samsun-Gabbro	**Easting** 266686	**Northing** 4569700													
		44.74	13.19	13.65	7.14	12.51	0.04	3.59	0.94	0.32	0.32	0.00	0.01	2.86	99.31	

Table 3- Major (wt%) element data of the Ordu beach sands and adjacent rocks.

Sampling site	Sample type and no	Easting 351215	Northing 4556355													
	Beach sand sample no	**SiO_2**	**Al_2O_3**	**Fe_2O_3**	**MgO**	**CaO**	**Na_2O**	**K_2O**	**TiO_2**	**P_2O_5**	**MnO**	**V_2O_5**	**Cr_2O_3**	**LOI**	**Sum**	**CIA**
Ordu-Ünye Cuma Stream (n=9)	UNC-01	51.75	14.27	7.42	2.29	10.39	1.93	2.53	0.63	0.21	0.12	0.03	0.01	7.78	99.36	37.01
	UNC-02	50.38	14.26	11.58	3.21	8.28	2.28	1.97	0.63	0.20	0.13	0.03	0.01	7.48	100.44	41.08
	UNC-03	50.18	14.01	9.12	3.17	8.31	2.27	2.06	0.53	0.19	0.12	0.03	0.03	9.88	99.88	40.45
	UNC-04	57.90	13.73	6.39	2.91	8.34	2.19	2.00	0.54	0.20	0.12	0.03	0.01	3.35	97.69	40.17
	UNC-05	48.83	12.49	16.55	4.47	9.44	1.88	1.67	0.56	0.18	0.14	0.03	0.03	3.97	100.24	36.60
	UNC-06	55.08	10.69	7.87	5.72	12.67	1.30	1.23	0.69	0.17	0.18	0.04	0.02	3.66	99.32	29.06
	UNC-07	50.69	10.97	17.16	5.26	11.02	1.05	1.34	1.15	0.20	0.19	0.06	0.03	0.65	99.76	32.56
	UNC-08	50.11	10.47	13.50	5.77	11.90	1.28	1.17	1.20	0.21	0.21	0.08	0.03	3.66	99.60	29.93
	UNC-09	54.80	11.32	10.75	4.85	10.73	1.22	1.38	0.97	0.19	0.18	0.06	0.02	3.65	100.11	33.41
Ordu-Ünye Ele Stream (n=4)		Easting 359692	Northing 4552801													
	ELE-01	59.16	13.46	7.33	2.12	9.92	1.81	2.43	0.61	0.20	0.12	0.03	0.00	2.47	99.67	36.74
	ELE-02	60.19	14.09	6.29	2.43	9.98	2.47	2.28	0.53	0.19	0.12	0.02	0.00	1.57	100.16	36.78
	ELE-03	57.83	13.65	5.99	2.38	10.43	2.21	2.07	0.48	0.18	0.14	0.02	0.00	4.04	99.43	35.87
	ELE-04	56.50	13.62	5.68	2.53	11.72	1.72	1.93	0.45	0.18	0.13	0.02	0.00	4.93	99.41	34.56
Ordu-Perşembe Akçaova Stream (n=8)		Easting 401607	Northing 4541771													
	AKC-01	59.95	13.74	7.05	2.58	7.71	1.68	3.66	0.61	0.22	0.11	0.03	0.02	1.93	99.28	40.45
	AKC-02	58.12	13.14	6.08	2.13	6.10	1.47	3.60	0.51	0.19	0.10	0.02	0.00	8.04	99.52	43.67
	AKC-03	56.32	13.91	12.25	3.08	6.58	1.58	3.32	0.79	0.17	0.14	0.04	0.00	1.94	100.11	43.92
	AKC-04	59.80	16.17	7.16	3.33	6.60	2.21	3.58	0.58	0.17	0.13	0.02	0.00	0.72	100.48	45.84
	AKC-05	62.42	13.76	6.28	2.19	6.50	1.75	3.87	0.54	0.22	0.10	0.02	0.00	2.59	100.24	42.83
	AKC-06	60.54	13.67	5.25	2.06	6.74	1.81	3.72	0.45	0.21	0.10	0.02	0.00	4.93	99.50	42.14
	AKC-07	57.82	13.42	9.53	3.01	8.41	1.13	2.87	0.87	0.19	0.15	0.05	0.00	2.55	99.99	40.39
	AKC-08	52.84	10.38	11.01	4.31	11.55	0.19	2.00	1.02	0.17	0.21	0.08	0.00	5.91	99.68	31.04
Sampling site	**Sample type and no**	**Easting** 415649	**Northing** 4537067													
	Beach Sand Sample no	**SiO_2**	**Al_2O_3**	**Fe_2O_3**	**MgO**	**CaO**	**Na_2O**	**K_2O**	**TiO_2**	**P_2O_5**	**MnO**	**V_2O_5**	**Cr_2O_3**	**LOI**	**Sum**	**CIA**
Ordu-Turnasuyu Stream (n=4)	TU-01	56.51	13.33	11.99	1.94	4.59	2.34	3.85	0.40	0.17	0.09	0.02	0.00	3.86	99.09	45.52
	TU-02	61.30	13.33	4.05	1.64	3.76	2.58	4.37	0.35	0.17	0.07	0.02	0.00	7.56	99.21	46.41
	TU-03	59.13	13.57	6.64	1.79	4.15	2.59	4.04	0.39	0.17	0.09	0.02	0.00	7.86	100.44	46.25
	TU-04	56.39	12.76	9.87	1.86	4.62	1.99	3.90	0.40	0.18	0.09	0.02	0.01	8.77	100.85	45.21
Adjacent Rock	**Ordu-Basalt**	**Easting** 395729	**Northing** 4525952													
		50.83	19.4	9.90	4.26	5.84	3.15	2.37	0.46	0.35	0.07	0.00	0.01	3.79	100.42	
	Ordu-Andesite	**Easting** 338830	**Northing** 4547102													
		54.44	15.26	11.14	5.88	6.70	3.55	2.22	0.73	0.36	0.10	0.01	0.00	0.28	100.65	

source rocks. In contrast to the Bartın region, SiO_2 contents of beach sand sampled from the Samsun and Ordu districts have moderately low and relatively high CaO concentrations, except for the Turnasuyu sample. Average Fe_2O_3 contents are quite high in the Ordu-Cuma Stream sands.

In the upper continental crust (UCC) normalized major oxide patterns (Figures 6a-6c), high concentrations of Fe_2O_3, TiO_2 and MnO observed in almost all the sand samples from the Samsun and Ordu sites supporting the presence of opaque Fe-Ti bearing minerals (Garzanti et al., 2015). In almost all

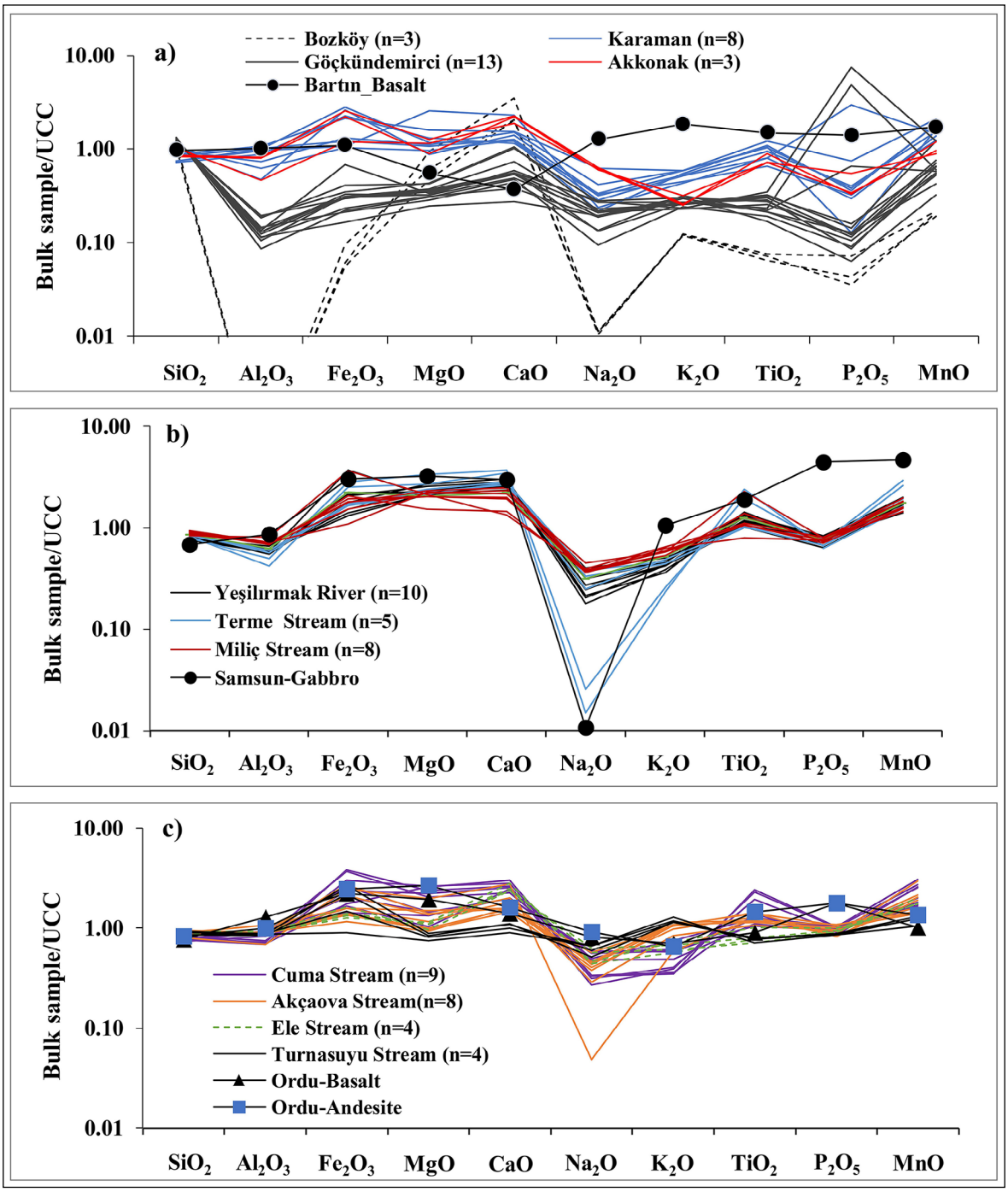

Figure 6- Bulk beach sands and adjacent host rocks major oxide composition in normalized Upper Continental Crust (UCC) diagrams (UCC: Taylor and McLennan, 1985); a) Bartın, b) Samsun, c) Ordu districts.

the regions, Na_2O depletion in samples might be due to the weathering effect on alkali metals. The abundance of pyroxene contributes to the enrichment of CaO and MgO (Garzanti et al., 2010). The comparison between geochemical compositions of four beach areas in Bartın region is quite distinctive from each other. Al_2O_3 and Na_2O contents of the bulk beach sand and basaltic rock reveal considerable differences and a significant decrease especially for the Bartın-Bozköy area. In the Bartın-Göçkündemirci site, P_2O_5 content is found quite high with respect to sands from other regions and the host basaltic rock as well. High CaO concentration of Bartın sand samples, even higher than the host rock, is attributed to derivation from the carbonate clastic units (Figure 6a).

Mobile alkali and alkaline earth metals are used to determine the weathering rates of components that form under different climate regimes. The geochemical variations recognized in the beach sands depend chiefly on mineralogical diversity (Nesbitt and Young, 1982; Nesbitt and Markovics, 1997; Garzanti and Resentini, 2016). The chemical compositions of clastic rocks provide information on the source rock mineralogy, which is exposed to chemical weathering before and after the deposition (Nesbitt and Young, 1982). Chemical index of alteration value calculated using relative molecular proportions of mobile alkali and alkaline major oxides with the equation of $CIA = [Al_2O_3/Al_2O_3 + Na_2O + CaO^* + K_2O)] \times 100$) (Nesbitt and Young, 1982), where CaO* represents the calcium concentration in silicates only (Nesbitt and Young, 1982). Depending on the degree of weathering in the source area, the concentrations of alkaline and alkaline earth elements in clastic sedimentary rocks are strongly affected by the alteration. The average CIA values of the Bartın (28.5, n=27), Samsun (29.5, n=22) and Ordu (40, n=25) beach sands are quite low. CIA values less than <50 indicate weak alteration on the source rocks. On the A-CN-K ternary diagram, all samples, except for Bartın-Karaman, plot along the A-CN axis and below the feldspar line (Figure 7) suggesting steady weathering conditions for the source rocks.

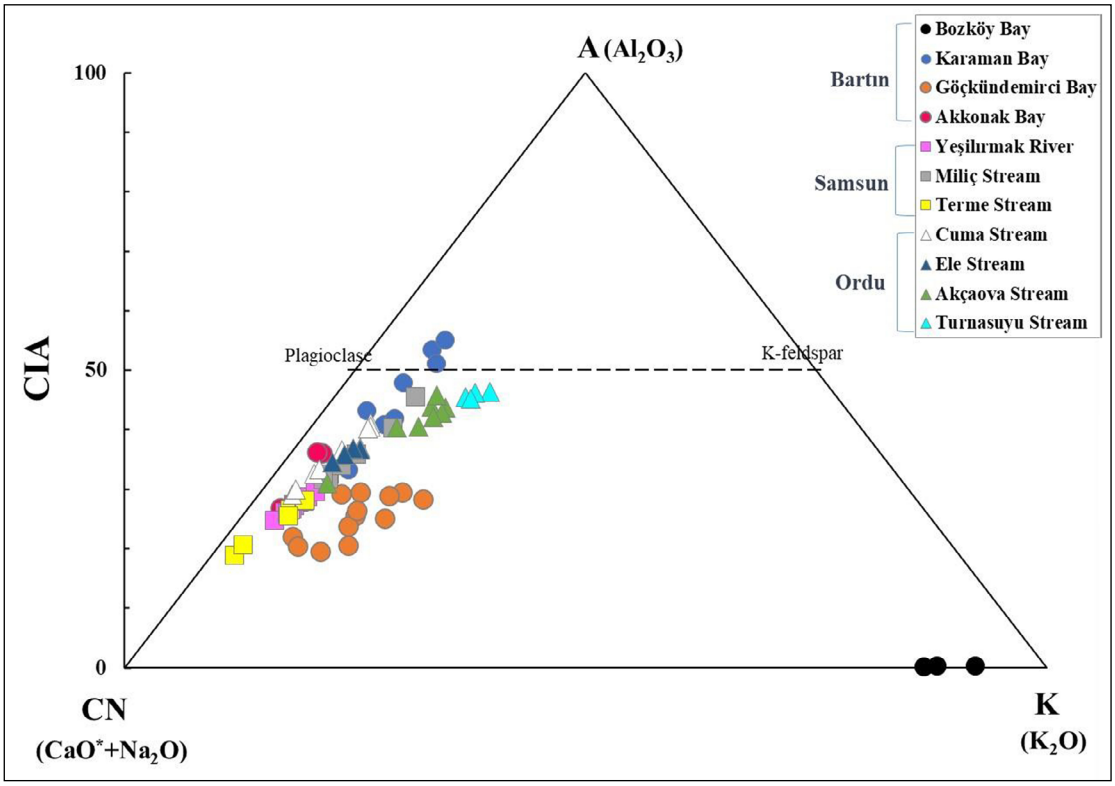

Figure 7- A-CN-K ternary diagram for the bulk beach sands from the western (Bartın) and eastern (Samsun-Ordu) coasts of the Black Sea region (the vertexes represent the molar proportions of $A=Al_2O_3$; $CN=CaO^*+Na_2O$; $K=K_2O$, and CIA: chemical index of alteration) (Nesbitt and Markovics, 1997).

4.3. Rare Earth Element Geochemistry of Bulk Beach Sands

In sandstones and terrigenous sediments, the relative abundances of detrital mineral assemblages are affected by transportation, deposition, and diagenesis processes. On the other hand, trace element concentrations of the mineral phases within the sediments, and the chemical composition of the source rock are not no remarkably changed (Taylor and McLennan, 1985; McLennan et al., 1993). For this reason, elements that behave immobile through the sedimentation cycle are very helpful for determining the geochemical characteristics of the source area (McLennan et al., 1983, 1990; Taylor and McLennan, 1985; Cullers, 1994).

The total REE+Y (∑REY) contents in samples from the Bartın, Samsun and Ordu districts vary from 30.9 to 162.1 ppm (Table 4). In the chondrite-normalized REE diagrams, studied beach sands from all locations show flat-type REE patterns that are significantly greater than the unity (Figure 8). The degree of enrichment for light REE (LREE) is higher by a factor of about 10 than heavy rare earth elements (HREE) for both beach sands and source rocks. The REY patterns of the samples show homogeneous trends nearly consistent with both basaltic and andesitic rocks in the Samsun and Ordu sites (Figures 8a-8c). However, the patchy anomaly between Dy and Y for the Bartın-basalt sample REY pattern may have been caused by analytical error (Figure 8a). The negative Eu (Eu/Eu*) anomalies (0.46 to 0.83) indicate derivation from mainly mafic type source rocks (Cullers, 1994, 2000; Armstrong-Altrin et al., 2012).

4.4. Elemental Chemistry of Magnetite Grains

EPMA analyses were conducted to determine concentrations of Mg, Ti, Cr, Al, Mn, Fe, Zn, Ni, V and Co on detrital magnetite grains selected from Samsun and Ordu beach sands (Figure 9). The representative results are presented as weight percentage of oxide (Table 5) and Fe recalculated as Fe_2O_3 and FeO following the procedure of Carmichael (1967). To determine the provenance of sediments, we used the triangle diagram of Grigsby (1990) that discriminates between mafic and intermediate magmatics. However, the application of this graphic (Figure 10) has some limitations and therefore, the multi-element diagram of Dare et al. (2014) was used for (Figure 11) further provenance studies.

According to the EPMA data, Fe_2O_3 contents (ave. Samsun: 56.3%wt; ave. Ordu: 56.7%wt) of the samples are significantly lower than a stoichiometric composition of magnetite (Fe_2O_3 68.9%) but FeO contents (ave. Samsun: 31.2%; ave. Ordu: 31.6%) are slightly higher than the stoichiometric value (FeO 31.04%). Magnetites of the Ordu-Cuma Stream and Samsun-Miliç districts are represented by relatively higher Al_2O_3 concentrations (ave. 4.29% and 5.12%. respectively). The high Cr_2O_3 contents are found in samples from the Samsun-Yeşilırmak and Ordu-Ele Stream areas (ave. 1.76% and 2%, respectively). Almost all the Samsun and Ordu samples have similar TiO_2 and V_2O_3 concentrations (with averages of 5.2% and 5.2%; 0.1% and 0.1%). The Ordu-Cuma Stream samples have high MnO contents (ave 1.08%). The highest (ave. 2.45%) and lowest (ave. 0.81%) MgO concentrations are recorded in Samsun-Miliç and Samsun-Terme samples, respectively. Ti and Al contents of >2% indicate that magnetites are of magmatic origin (Firouzi et al., 2024).

Elemental concentrations of detrital magnetites are plotted on a triangular TiO_2-Fe_2O_3-FeO diagram (Figure 10). Studied opaque minerals with similar chemical compositions fall into the 50% magnetite field of the ulvospinel-magnetite series. Mineral chemistry of investigated magnetites is consistent with intermediate volcanic and mafic plutonic rocks (Grigsby, 1990). Ti^{4+} within the magnetites replaces Fe^{3+}, especially in intermediate volcanic and mafic rocks, which results in a negative correlation between Fe_2O_3 and TiO_2 and a positive correlation between FeO and TiO_2 (Basu and Molinaroli, 1989; Grigsby, 1990; Deer et al., 1992; Razjigaeva and Naumova, 1992). Aluminum generally replaces for Cr and V substitutes Fe^{3+} and Fe^{2+} is replaced by Ca, Mg, Mn, Ni, Co and Zn (Deer et al., 1992). The fact that Fe_2O_3 concentration of the studied samples is lower than the stoichiometric composition of magnetites can be explained by the relatively high concentrations of Al, Cr and V. The low concentrations of Mg, Mn, Ni,

Table 4- REE element data for the studied beach sand sediments (ppm).

Location	Sample No	La	Ce	Pr	Nd	Sm	Eu	Gd	Tb	Dy	Y	Ho	Er	Tm	Yb	Lu	∑REY	Eu/Eu*
Bartın-Bozköy Bay	BRT-03	6.60	11.50	1.35	5.20	0.90	0.17	0.80	0.10	0.62	3.00	0.10	0.35	-	0.20	0.04	30.93	0.61
Bartın-Karaman Bay	BRT-10	13.50	23.60	3.19	12.50	2.90	0.56	2.50	0.37	3.22	16.20	0.61	1.89	0.23	1.50	0.27	83.04	0.63
	BRT-04	9.20	15.80	2.06	8.70	2.00	0.43	1.90	0.27	2.29	11.30	0.42	1.32	0.15	1.00	0.18	57.02	0.67
Bartın-Göçkündemirci Bay	BRT-23	9.00	17.30	1.99	7.40	1.50	0.29	1.20	0.16	1.11	5.30	0.20	0.64	0.07	0.50	0.08	46.74	0.66
	BRT-37	8.20	15.00	1.72	6.10	1.10	0.25	1.00	0.13	0.86	4.20	0.16	0.49	0.06	0.40	0.06	39.73	0.73
Bartın-Akkonak Bay	BRT-40	11.10	19.90	2.60	10.50	2.40	0.61	2.10	0.30	2.61	13.60	0.49	1.56	0.18	1.20	0.22	69.37	0.83
Samsun-Yeşilırmak River	SY-01	19.10	35.40	4.31	17.90	3.90	0.71	3.50	0.45	3.62	16.70	0.61	1.93	0.21	1.50	0.24	110.08	0.59
	SY-02	21.10	39.30	4.76	19.90	4.20	0.74	3.60	0.49	3.80	17.80	0.66	2.03	0.22	1.50	0.25	120.35	0.58
	SY-03	16.00	30.80	3.82	16.60	3.70	0.67	3.40	0.44	3.55	16.80	0.63	1.92	0.21	1.40	0.25	100.19	0.58
	SY-04	18.80	34.60	4.26	18.00	4.00	0.73	3.40	0.47	3.48	17.10	0.63	2.06	0.21	1.40	0.25	109.39	0.60
	SY-05	15.80	30.30	3.80	16.40	4.00	0.74	3.40	0.47	3.73	17.40	0.65	1.89	0.21	1.40	0.24	100.43	0.61
	SY-06	16.50	31.00	3.88	17.00	3.90	0.72	3.40	0.45	3.52	16.90	0.64	1.93	0.20	1.40	0.24	101.68	0.60
	SY-07	20.40	37.00	4.72	20.00	4.30	0.79	3.80	0.49	3.72	18.20	0.68	2.08	0.22	1.50	0.27	118.17	0.60
	SY-08	18.90	34.60	4.16	17.20	3.60	0.70	3.20	0.41	3.29	15.20	0.57	1.73	0.20	1.30	0.23	105.29	0.63
Samsun-Terme Stream	ST-01	25.70	47.00	5.61	23.30	5.10	0.77	4.60	0.59	4.74	23.00	0.82	2.52	0.27	1.90	0.31	146.23	0.48
	ST-02	29.00	53.90	6.33	25.80	5.70	0.80	5.00	0.64	5.01	23.80	0.87	2.71	0.28	1.90	0.33	162.07	0.46
	ST-03	20.00	36.90	4.42	18.50	4.10	0.69	3.40	0.45	3.62	17.40	0.63	1.90	0.22	1.40	0.26	113.89	0.56
Samsun-Miliç Stream	SM-01	20.80	36.50	4.37	17.40	3.50	0.74	2.90	0.38	2.91	13.70	0.52	1.61	0.18	1.30	0.23	107.04	0.71
	SM-02	20.40	36.40	4.42	18.30	4.00	0.74	3.40	0.42	3.46	16.40	0.60	1.85	0.21	1.30	0.24	112.14	0.61
	SM-03	18.10	32.60	3.94	16.70	3.80	0.71	3.20	0.41	3.09	15.60	0.56	1.75	0.20	1.30	0.24	102.20	0.62
	SM-04	20.20	35.20	4.13	16.60	3.60	0.73	3.00	0.38	2.93	14.60	0.53	1.69	0.19	1.20	0.22	105.20	0.68
	SM-05	20.70	35.90	4.29	16.80	3.50	0.75	2.80	0.36	2.75	13.70	0.48	1.52	0.17	1.20	0.22	105.14	0.73
	SM-07	22.60	42.40	5.00	20.10	4.20	0.82	3.50	0.46	3.50	17.20	0.60	1.93	0.20	1.40	0.25	124.16	0.65
Ordu-Ünye-Cuma Stream	UNC-01	23.70	42.70	5.01	19.90	3.90	0.80	3.30	0.44	3.46	17.30	0.62	2.01	0.22	1.50	0.27	125.13	0.68
	UNC-02	19.50	35.20	4.32	17.70	3.80	0.81	3.10	0.40	3.09	15.30	0.56	1.76	0.20	1.30	0.23	107.27	0.72
	UNC-03	20.00	36.60	4.50	18.60	3.90	0.84	3.40	0.42	3.16	15.60	0.57	1.85	0.21	1.30	0.25	111.20	0.70
	UNC-04	18.90	34.10	4.17	17.60	3.70	0.80	3.20	0.40	3.09	15.50	0.56	1.70	0.20	1.30	0.25	105.47	0.71
	UNC-05	17.40	33.20	4.25	18.90	4.30	0.84	3.70	0.48	3.80	17.80	0.66	1.99	0.22	1.50	0.26	109.30	0.64
	UNC-06	15.90	32.60	4.39	20.40	4.90	0.85	4.10	0.55	4.29	21.00	0.77	2.30	0.26	1.70	0.30	114.31	0.58
	UNC-07	20.10	39.40	4.94	21.80	4.70	0.80	4.00	0.51	4.01	19.70	0.73	2.20	0.24	1.60	0.29	125.02	0.56
	UNC-08	16.60	34.80	4.66	21.20	5.10	0.81	4.20	0.55	4.35	21.10	0.76	2.36	0.26	1.70	0.30	118.75	0.53
	UNC-09	15.70	31.90	4.22	18.80	4.40	0.81	3.70	0.47	3.82	18.50	0.67	2.06	0.23	1.50	0.27	107.05	0.61
Ordu-Ünye-Ele Stream	ELE-01	24.90	44.60	5.23	21.20	4.40	0.82	3.50	0.46	3.51	18.00	0.63	2.04	0.23	1.60	0.29	131.41	0.64
	ELE-04	19.90	36.10	4.30	17.70	3.80	0.80	3.30	0.43	3.43	16.20	0.57	1.79	0.21	1.40	0.26	110.19	0.69
Ordu-Perşembe-Akçaova Stream	AKC-03	27.20	48.70	5.96	23.50	5.00	0.92	4.10	0.54	4.24	21.20	0.77	2.45	0.27	1.90	0.33	147.08	0.62
	AKC-04	25.30	46.30	5.64	22.30	4.70	0.95	4.10	0.53	4.09	20.50	0.74	2.39	0.26	1.80	0.32	139.92	0.66
	AKC-06	31.50	52.30	6.43	25.00	5.00	1.00	4.20	0.55	4.21	21.00	0.73	2.40	0.28	1.80	0.34	156.74	0.67
	AKC-08	19.10	37.70	5.10	22.90	5.90	0.92	5.20	0.68	5.74	27.20	1.00	3.05	0.35	2.30	0.41	137.55	0.51
Ordu-Turnasuyu Stream	TU-01	32.40	55.20	6.41	24.00	4.60	0.93	3.70	0.47	3.44	17.40	0.63	2.06	0.23	1.60	0.28	153.35	0.69
	TU-02	33.00	55.00	6.43	23.20	4.20	0.87	3.40	0.41	3.20	15.70	0.55	1.83	0.20	1.50	0.27	149.76	0.70
Adjacent Rocks	Bartın-Basalt	18.70	42.10	5.79	22.40	5.20	0.76	4.10	0.62	3.95	23.30	0.92	1.65	0.40	2.50	0.46	132.85	0.30
	Samsun-Gabbro	42.90	102.0	13.70	54.90	13.40	0.43	9.40	1.35	8.14	1.82	3.13	0.78	4.80	0.85	44.40	302.00	0.37
	Ordu-Basalt	25.70	53.90	6.62	24.20	4.40	0.70	3.90	0.45	0.87	0.42	0.87	0.16	1.00	0.19	9.80	133.18	0.37
	Ordu-Andesite	45.80	92.00	10.50	37.20	6.30	0.72	5.80	0.67	1.21	0.57	1.21	0.22	1.30	0.23	13.30	217.03	0.37

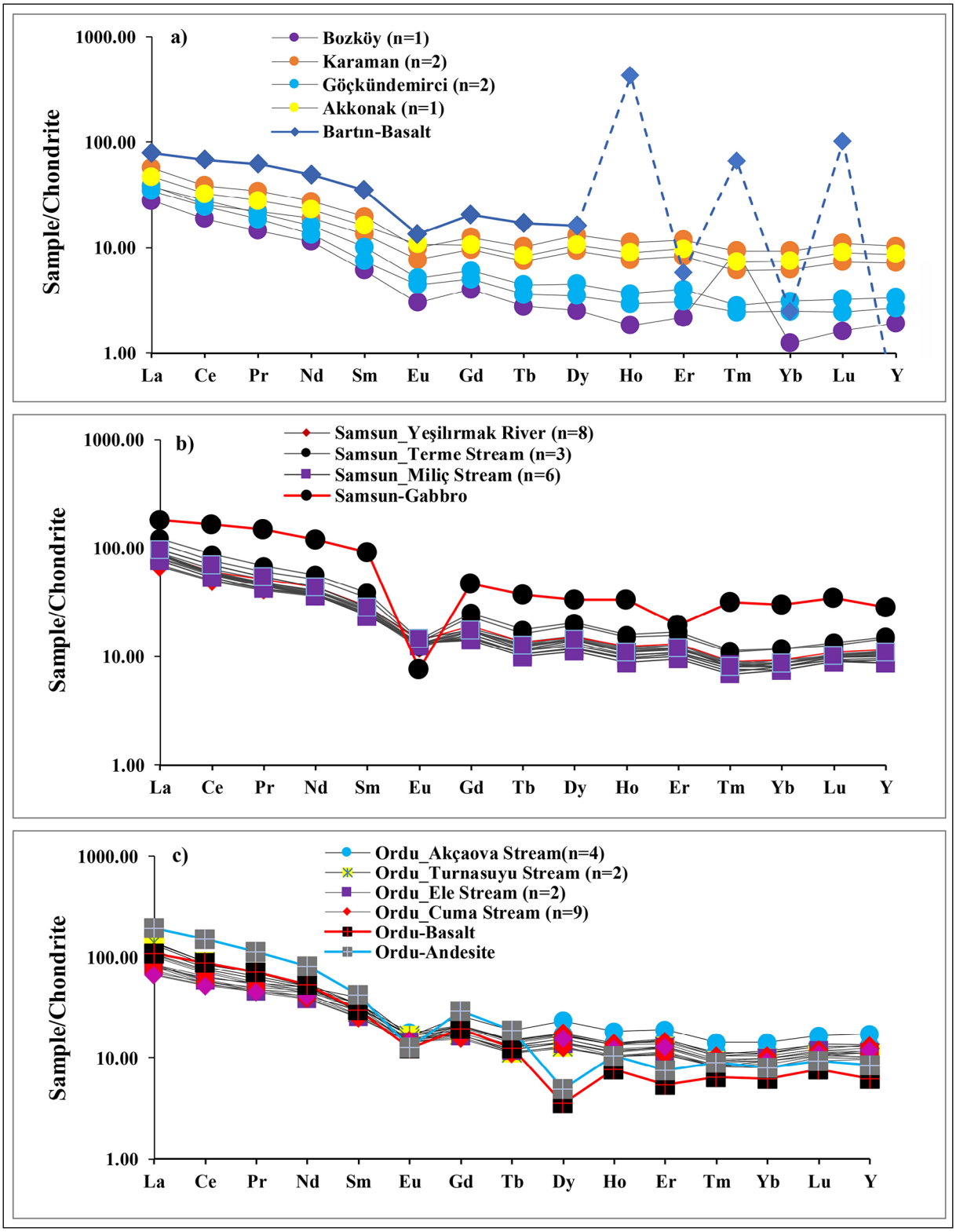

Figure 8- Bulk beach sands and adjacent host rocks chondrite-normalized REY patterns (McDonough and Sun, 1995) a) Bartın-Bozköy; Karaman; Göçkündemirci and Akkonak, b) Samsun-Yeşilırmak; Terme; Miliç, c) Ordu-Akçaova; Ele; Cuma and Turnasuyu Streams.

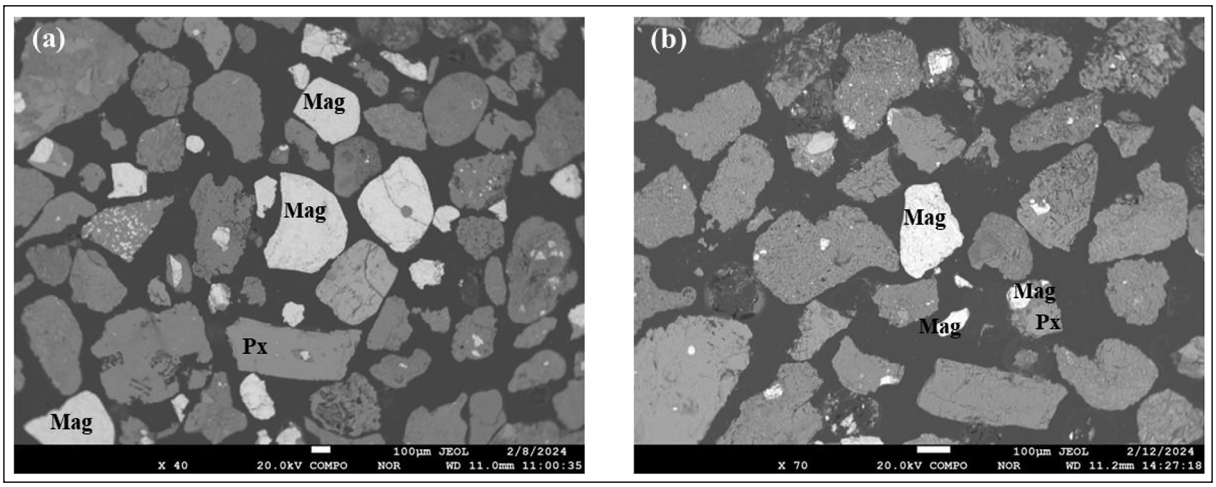

Figure 9- Back-scattered (BSE) images representing detrital magnetite minerals from (a) Samsun and (b) Ordu districts.

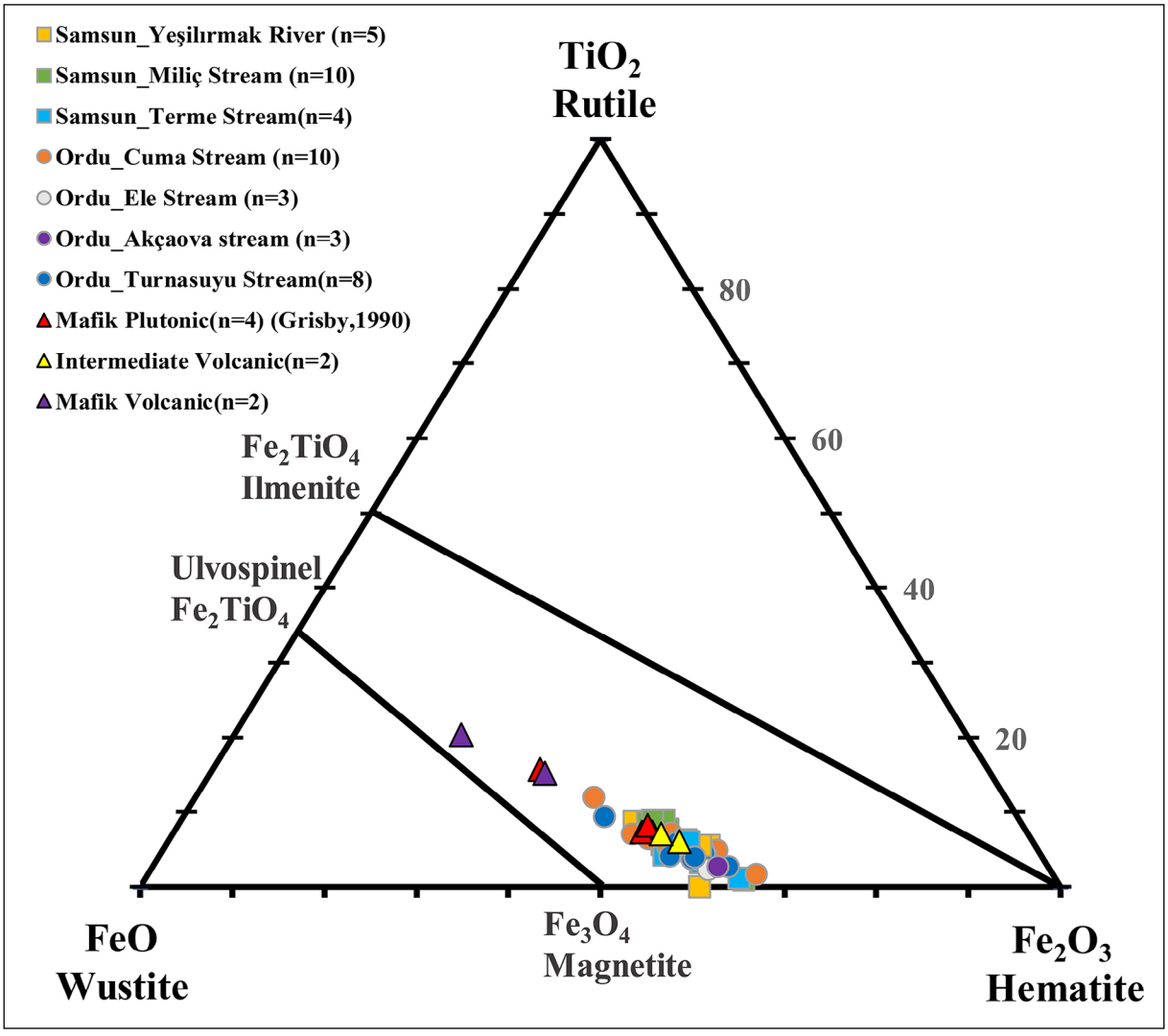

Figure 10- Major elemental compositions of detrital magnetite grains on a ternary plot showing boundaries of various Fe-Ti oxides (Carmichael, 1967).

Table 5- Representative EPMA analysis results of magnetite from Samsun and Ordu district (TOT: total; r: rim; c: core; Mag: Magnetite; Hem: Hematite) (Formula calculated based on 4 Oxygen).

	Samsun					Ordu		
	r	r	c	r	r	r	c	r
MgO	2.80	3.12	3.23	3.54	3.26	0	0.14	0.04
Al_2O_3	5.75	5.15	5.91	5.63	7.76	0.62	4.28	5.97
Cr_2O_3	0.01	0.02	0	0.03	0.02	0.03	0.02	0.01
FeO(tot)	84.26	85.18	80.06	82.04	74.17	85.53	83.09	82.42
V_2O_3	0.15	0.19	0.18	0.2	0.16	0	0.09	0.17
SiO_2	0.13	0.11	0.11	0.11	0.18	0.37	0.49	0.13
TiO_2	5.57	5.52	5.55	5.74	5.7	4.38	5.35	6.56
MnO	0.41	0.34	0.42	0.43	0.37	0.012	0.00	0.03
NiO	0.17	0.47	0.28	0	0	0.01	0	0
ZnO	0.02	0.04	0.02	0.02	0	0.03	0.07	0.05
TOT	99.27	100.14	95.78	97.74	91.63	90.98	93.56	95.38
Mineral phase	Mag	Mag	Mag	Mag	Hem	Mag	Mag	Hem
Mg	0.2	0.2	0.2	0.2	0.2	0	0	0
Al	0.3	0.3	0.3	0.3	0.4	0.02	0.18	0.25
Cr	0	0	0	0	0	0	0	0
Fe^{2+}	0.94	0.95	0.92	0.93	0.86	1.11	1.07	1.07
Fe^{3+}	1.88	1.91	1.85	1.87	1.73	1.7	1.56	1.44
V	0	0	0	0	0	0	0	0
Si	0	0	0	0	0	0.01	0.01	0
Ti	0.2	0.2	0.2	0.2	0.2	0.12	0.12	0.18
Mn	0	0	0	0	0	0	0	0
Ni	0	0	0	0	0	0	0	0
Zn	0	0	0	0	0	0	0	0
Total	3.52	3.56	3.47	3.5	3.39	2.96	2.94	2.94

Co and Zn (<1%) might indicate that these elements replace Fe^{2+} at a small extent.

4.5. Trace Elements in Magnetite

Spinel group minerals, such as magnetite, are quite stable under low temperature and pressure conditions during the mechanical and chemical weathering (Morton, 1991). They are found in a wide variety of sedimentary environments (Pettijohn et al., 1987; Grigsby, 1990). Magnetites within the mafic-ultramafic interlayered magmatic ore deposits (Fe-Ti-V) that crystallized from high-temperature silicate magmas preserve their primary form. They are also recognized as an accessory mineral in magmatic-hydrothermal systems, hydrothermal systems, porphyry and skarn-type ore zones and magmatic and metamorphic rocks. Processes controlling the trace element partitioning in magnetite minerals derived from different sources have been widely used especially in ore mineralogy and sedimentology studies to investigate the provenance and petrogenetic characteristics (Basu and Molinaroli, 1989; Grigsby, 1990; Razjigaeva and Naumova, 1992; Yang et al., 2009; Dupuis and Beaudoin, 2011; Nadoll et al., 2012; Dare et al., 2014).

In multi-element diagrams (Figures 11a and 11b), trace element contents (Si, Ca, Y, P, Pb, Zr, Hf, Al, Ge, W, Sc, Ta, Nb, Cu, Mo, Sn, Ga, Mn, Mg, Ti, Zn, Co, V, Ni, and Cr) were normalized with respect to bulk continental crust values (Rudnick and Gao, 2003) in the order of increasing element compatibility with magnetite (Dare et al., 2014). Trace element concentrations of magnetites determined by EPMA analyses were compared with those of magnetite

phenocrysts within andesitic rocks of intermediate composition and primary massive magnetites of the Bushveld Complex (Fe-Ti-V deposits) (Dare et al., 2014).

The element concentrations of magnetite minerals that fractionated from a high-temperature silicate magma depend on factors such as the magma composition, temperature, pressure, oxygen fugacity and cooling rate of the melt as well as the partition coefficient of minerals precipitated simultaneously with magnetites from the melt (Spencer and Lindsley, 1981; Ghiorso and Sack, 1991; Mollo et al., 2013; Dare et al., 2014). During the separation of intermediate and mafic melts from the same type of magma, Ni and Cr concentrations of the silicate melt decrease while mafic minerals such as pyroxene and magnetite continue to be fractionated.

Trace element concentrations of the studied magnetites show similar patterns. Irregular changes and low concentrations were observed in Si, Ca, P, Y, Zr and Pb that behave in an incompatible manner with respect to magnetite (Figures 11a and 11b). High concentrations of P can be explained by the presence of inclusions (e.g. apatite) in magnetite (Duparc et al., 2016). Elements that are compatible with magnetite (e.g. Mg, Co, Ni, V and Cr) are highly enriched in massive magnetites within orthomagmatic Fe-Ti-V type deposits (Dare et al., 2014) but concentrations of these elements in the studied magnetites are quite low (Figures 11a and 11b). Elements that are incompatible

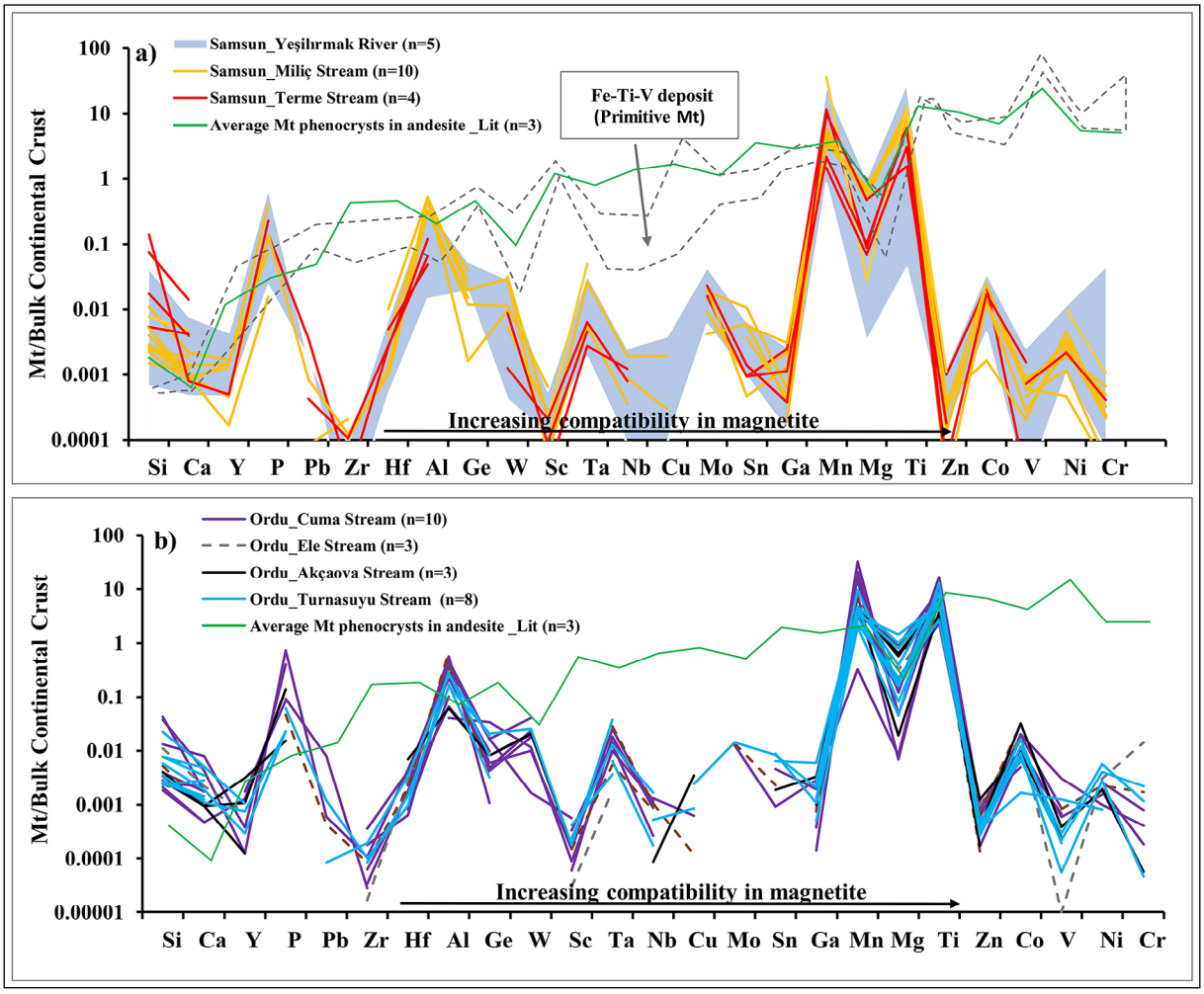

Figure 11- Multi-element variation diagrams with increasing element compatibility for eastern Black Sea detrital magnetites (After Dare et al., 2014). Normalization values are from Rudnick and Gao (2003). a) Samsun magnetite samples. b) Ordu magnetite samples. Data for magnetite from average Mt phenocrysts and Fe-Ti-V (primitive Mt) magnetite from Dare et al. (2014). n: Total number of analyzed magnetites (Mt).

with magnetite (e.g. Hf, Ga, Ge, W, Sc, Mo, Nb, Sn, Ta) have relatively low concentrations in the magnetites from the Samsun and Ordu regions. The Mn and Ti (elements compatible with magnetite) patterns of the studied magnetites are consistent with the magnetites found in andesitic and Fe-Ti-V deposits (Dare et al., 2014).

5. Discussion

5.1. Depositional Factors Affecting Opaque Heavy Mineral Layers

Coastal or beach placer deposits are concentrations of heavy minerals mechanically eroded from the exposed adjacent rocks. A turbulent regime, including current and wave action, carries the suspended sand towards the beach. When a wave breaks, the sand grains settle momentarily. Only light minerals can be entrained by the flow back to the sea. Heavy minerals are enriched in a narrow linear band along the beach (Pohl, 2005). Placer formation can also be caused by other coastal processes such as tides, currents, wind and storms.

Coastal and littoral currents or storm waves carry significant amounts of HM-bearing sediments to the beach area. In the Bartın region, as the sea level rises around the coast during the transgression period, sediments are delivered to the beaches. Lagoons or embayments located behind the shoreline may act as a transgressive barrier for the accretionary area (Figures 2a-2e). Thus, bay-linked areas of sediment accumulation are controlled by littoral and tidal currents on the shoreline (Roy, 1984; Hou et al., 2017).

For the Samsun and Ordu beaches, the accumulation areas appear as sheltered shorelines with a medium slope or inclination of the pre-existing land surface adjacent to the shoreline fed by approximately N-S oriented rivers and streams connected to the coastal or deltaic environment and drainages from HM-bearing areas. As a result, during transgression/ regression or storms, substantial proportion of HM-bearing zones in the sand, particularly lighter components such as quartz are carried along the shore by littoral or wave dominated drift while high density components (Figures 2ı and 2j) tend to concentrate in lag or onshore sites (Hou et al., 2017). The abundance of heavy minerals such as magnetite may vary with seasonal turnaround.

In previous studies, it was pointed out that river discharges exert a great control on beach sand composition (Armstrong-Altrin et al., 2012). Our observations also indicate that petrographic and geochemical changes in the sand samples along the Samsun and Ordu beach areas are largely controlled by the type of sediments transported by the Yeşilırmak, Miliç and Melet rivers, respectively. Distribution of beach sediments along these provinces is controlled by the fluvial effects. On the contrary, Bartın bays receive sediments from different source areas. For this reason, determining the geochemical composition of beach sand is likely more important than the grain size distribution. However, the major geochemical parameters might change gradually with the increase or decrease in the mean grain size (e.g. Armstrong-Altrin et al., 2012). Moreover, hydraulic sorting does not have an effect on determining the provenance of the sediments.

There are many porphyry Cu-Mo-Au ore deposits in Samsun (Yiğit, 2009) and principally small Fe and Fe-Cu-skarn ore bodies such as Ordu-Kertiliyayla and Çambaşı provinces known to have important resources in the porphyry belt of the "Pontide Magmatic Arc", which is a very large magmatism area related to the Pontides (Kuşçu, 2019). In spite of the fact that the impact of these mining activities in region, even not very close to the study area, on the coastal accumulation areas should also be taken into consideration.

5.2. Comparison of Major Oxide Data

The CIA value is equivalent to the A value in the A–CN–K ternary diagram. In general, sediments derived from terrigenous sources with CIA values close to 50 are considered to be fresh or unaltered, those with CIA values around 75 are regarded moderately weathered, and those with CIA values close to 100 are considered to be subject to extreme chemical weathering. The triangle diagram was constructed with the understanding that CIA values are primarily controlled by Ca and Al contents (Fedo and Babechuk, 2023).

The calculated CIA values of bulk beach sands are presented in Tables 1, 2, 3 and the A-CN-K diagram (Figure 6). The lowest CIA values were determined in Bartın-Bozköy samples, while the highest CIAs were observed in Bartın-Karaman, Ordu-Akçaova and Turnasuyu sand samples. Regarding studied samples, CIA values were <55, indicating the rate of chemical weathering on beach sands is very slow or insignificant. These might indicate that studied beach sands experienced very low levels of weathering and may not be transported and deposited far from the source areas. The fact that almost all beach sand samples are located close to the CN axis confirms the relatively low degree of alteration or this is because the study area is dominated by weathering products of K-poor protolith rocks such as mafic igneous basaltic, gabbroic and/or calcic sedimentary protoliths and therefore parallel to CN axis (Algeo et al., 2025). However, Bartın-Bozköy samples imply that the depletion of Ca and Na-bearing silicate minerals from the source rocks or the effect of erosion in the drainage basin is more pronounced for the Ca-Na silicate minerals (Figure 7) (Li and Yang, 2010).

Major oxides and CIA ternary diagrams may be very helpful for evaluating the weathering profile of felsic or mafic source rocks. The relatively high SiO_2 concentrations of samples from the Bartın region might be derived from nearby volcanic and sedimentary clastics and explained by the resistance to weathering conditions. Ca contents of Bartın sand samples are quite low but those of Samsun and Ordu samples are high probably indicating a contribution of carbonate clastics, which are adjacent to the beach areas. Al and Na depletion accompanied by K-enrichment in all the studied bulk beach sands and mafic source rocks might demonstrate the plagioclase weathering, while almost all samples have negative Eu anomaly (Taylor and McLennan, 1985; McLennan and Taylor, 1991) (Figures 6a-6c). The fact that Na concentrations of beach sands are lower than their source rocks may be explained by the effect of alteration that occured much later than the crystallization of protolith. The advanced stage of weathering is characterized by a decrease in K_2O as the composition of weathered rocks approaches that of kaolinite and/or gibbsite (Nesbitt and Young, 1984).

Contrary to the behavior of felsic rocks, Mg is a key component for the instability of mafic rocks. Although Fe and Mg are labile cations and leachable from mafic components under an anoxic environment, Fe_2O_3 contents of the Samsun and Ordu sand samples are quite high. The presence of gabbroic and basaltic rocks along the paths of the streams significantly affect the Fe_2O_3 contents of Samsun and Ordu beach sands. Ca- and Mg-rich clinopyroxene and Fe-Ti oxides are important sources of Si, Mg and Fe contents of Samsun and Ordu samples. High CaO and MgO concentrations might also be explained by the accumulation of diopside at the beach site together with carbonaceous marine components and clastic carbonate rocks fragments.

5.3. Magnetite Mineral Chemistry

TiO_2-FeO-Fe_2O_3 triangle diagram indicates that the studied magnetites are of titanomagnetite composition since they closely plot to the ulvospinel-magnetite line. The high-temperature ulvospinel-magnetite series is the most basic Fe-Ti phase, especially in igneous rocks (Nagata, 1961). Titanium-rich magnetite can be oxidized to hematite or reduced in some cases (O'Reilly, 1984), which indicates a change in the stoichiometric composition. The magnetite is partly hematitized by the process of deuteric alteration. It may be formed in igneous or metamorphic rocks as a result of high-temperature deuteric alteration, or low-temperature oxidation during transportation. If it occurs in the source rock or is oxidized during the alluviation, the composition of the residual magnetite grains after deposition will be quite different. This chemical behavior is related to the temperature and redox conditions during the crystallization phase of the iron-rich silicate melt. The elemental distribution of magnetites is important in controlling the oxidation of the magma, the prevalence of ferric-ferrous iron, and the Ti content (Velasco et al., 2016). Although the overall chemical composition of magnetite is almost similar, core to rim differences in the mineral chemistry of magnetites yield the effect of alteration process (e.g. oxidation of magnetite to hematite) (Table 5).

6. Conclusion

Our recent geochemical and petrological data (after Köksoy, 1973) characterize Fe-rich heavy mineral sands between Samsun and Ordu coasts along the Black Sea. Beach sand sediment was systematically sampled from the eastern and western onshore sites of the Black Sea region where mainstream and major tributaries drained into the sea. According to the petrographic observations and chemical analysis results, the mineral assemblage contained in the beach sediments variable from east to western part of the study area and detrital magnetite found as dispersed grains in the matrix of volcanic rock fragments, as inclusions in pyroxene phenocrysts and as liberated grains. CIA values and A-CN-K ternary diagrams indicate that beach sands have undergone low-grade chemical alteration. Weathering of rock-forming minerals is incomplete during transport processes, probably because the depositional environments are close enough to the source rocks.

In the bulk sand fraction, the abundance and Fe_2O_3 content of magnetite from the Ordu-Cuma Stream and Samsun - Terme samples are much higher than Samsun - Yeşilırmak - Miliç, Ordu - Ele - Akçaova - Turnasuyu streams and Bartın samples. In-situ chemical analysis results reveal that magnetites are derived from mafic plutonic and volcanic rocks of intermediate composition. However, the results from this study indicate that magnetite in beach sands is susceptible to hydrothermal replacement and/or secondary Fe-oxide formation. The dissolution-redeposition process can lead to the occurrence of multiple generations of magnetite with different compositions in a single grain.

Acknowledgments

This study was supported by 100/2000 YÖK Scholarship Program. The Ankara University is acknowledged for the financial support (Grant No: FDK-2022-2529). Thanks, are also given to Yusuf Kağan Kadıoğlu and Kıymet Deniz Yağcıoğlu (Ankara University, Earth Science Research and Application Centre; YEBIM) for the field excursion, mineralogical insights and chemical analysis support. Authors are also grateful to Cüneyt Şen and three anonymous reviewers for their critical comments that greatly improved the manuscript.

References

Abdel-Karim, A. A. M., Barakat, M. G. 2017. Separation, upgrading, and mineralogy of placer magnetite in the black sands, northern coast of Egypt. Arabian Journal of Geosciences 10(14), 1-17.

Aksay, A., Pehlivan, Ş., Gedik, İ., Bilginer, E., Duru, M., Akbaş, B., Altun, İ. 2002. 1/500000 Scale Geological Inventory Map Series of Turkey, Zonguldak sheet, General Directorate of Mineral Research and Exploration, Ankara.

Algeo, T. J., Hong H., Wang C. 2025. The chemical index of alteration (CIA) and interpretation of ACNK diagrams. Chemical Geology 671, 122474.

Armstrong-Altrin, J. S., Lee, Y. I., Kasper-Zubillaga, J. J., Carranza-Edwards, A., Garcia, D., Eby, G. N., Cruz-Ortiz, N. L. 2012. Geochemistry of beach sands along the western Gulf of Mexico, Mexico: implication for provenance. Geochemistry 72(4), 345-362.

Basu, A., Molinaroli, E. 1989. Provenance characteristics of detrital opaque Fe-Ti oxide minerals. Journal of Sedimentary Research 59, 922-934.

Carmichael, I. S. E. 1967. The iron-titanium oxides of salic volcanic rocks and their associated ferromagnesium silicates. Contributions to Mineralogy and Petrology 14, 36-64.

Cullers, R. L. 1994. The controls on the major and trace element variation of shales, siltstones, and sandstones of Pennsylvanian-Permian age from uplifted continental blocks in Colorado to platform sediment in Kansas, USA. Geochimica et Cosmochimica Acta 58(22), 4955-4972.

Cullers, R. L. 2000. The geochemistry of shales, siltstones and sandstones of Pennsylvanian-Permian age, Colorado. USA: Implications for provenance and metamorphic studies. Lithos 51, 181-203.

Dare, S. A., Barnes, S. J., Beaudoin, G., Méric, J., Boutroy, E., Potvin-Doucet, C. 2014. Trace elements in magnetite as petrogenetic indicators. Mineralium Deposita 49, 785-796.

Deer, W. A., Howie, R. A., Zussman, J. 1992. An Introduction to The Rock-forming Minerals. Second ed. Longman Scientific and Technical. Hong Kong, 696.

Dill, H. G., Goldmann, S., Cravero, F. 2018. Zr-Ti-Fe placers along the coast of NE Argentina: Provenance analysis and ore guide for the metallogenesis in the South Atlantic Ocean. Ore Geology Reviews 95, 131-160.

Duparc, Q., Dare, S. A., Cousineau, P. A., Goutier, J. 2016. Magnetite chemistry as a provenance indicator in Archean metamorphosed sedimentary rocks. Journal of Sedimentary Research 86(5), 542-563.

Dupuis, C., Beaudoin, G. 2011. Discriminant diagrams for iron oxide trace element fingerprinting of mineral deposit types. Mineralium Deposita 46, 319-335.

Fedo, C. M., Babechuk, M. G. 2023. Petrogenesis of siliciclastic sediments and sedimentary rocks explored in three-dimensional Al_2O_3-CaO*+ Na_2O-K_2O-FeO+ MgO (A-CN-K-FM) compositional space. Canadian Journal of Earth Sciences 60(7), 818-838.

Firouzi, E., Ehya, F., Aliabadi, M. A., Mohammadi, R. 2024. Trace element geochemistry of magnetite from the Mahura iron placer deposit, Markazi province, Iran: implications for magnetite provenance rocks. Carbonates and Evaporites 39(3), 82.

Force, E. R. 1976. Metamorphic source rocks of titanium placer deposits - a geochemical cycle: U.S. Geological Survey Professional Paper, 959-B, 16.

Force, E. R. 1991. Geology of titanium-mineral deposits. Geological Society of America Special Paper, 259, 112.

Ergin, M., Karakaş, Z. S., Tekin, E., Eser, B., Sözeri, K., Çopuroğlu, İ., Koç, Ş., Şimşek, B. 2018. Provenance discrimination among foreshore, backshore, and dune environments in the black sand beaches along the Samandağ/Hatay coasts, SE Turkey (E Mediterranean). Arabian Journal of Geosciences 11, 1-20.

Garzanti, E., Andò, S. 2007. Heavy mineral concentration in modern sands: Implications for provenance interpretation. Developments in Sedimentology 58, 517-545.

Garzanti, E., Resentini, A. 2016. Provenance control on chemical indices of weathering (Taiwan river sands). Sedimentary Geology 336, 81-95.

Garzanti, E., Andò, S., France-Lanord, C., Vezzoli, G., Censi, P., Galy, V., Najman, Y. 2010. Mineralogical and chemical variability of fluvial sediments: 1. Bedload sand (Ganga–Brahmaputra, Bangladesh). Earth and Planetary Science Letters 299(3-4), 368-381.

Garzanti, E., Andò, S., Vezzoli, G., Lustrino, M., Boni, M., Vermeesch, P. 2012. Petrology of the Namib Sand Sea: Long-distance transport and compositional variability in the wind-displaced Orange Delta. Earth-Science Reviews 112(3-4), 173-189.

Garzanti, E., Padoan, M., Andò, S., Resentini, A., Vezzoli, G., Lustrino, M. 2013. Weathering and relative durability of detrital minerals in equatorial climate: sand petrology and geochemistry in the East African Rift. The Journal of Geology 121(6), 547-580.

Garzanti, E., Resentini, A., Andò, S., Vezzoli, G., Pereira, A., Vermeesch, P. 2015. Physical controls on sand composition and relative durability of detrital minerals during ultra-long distance littoral and aeolian transport (Namibia and southern Angola). Sedimentology 62(4), 971-996.

Ghiorso, M. S., Sack, O. 1991. Fe–Ti oxide geothermometry: Thermodynamic formulation and the estimation of intensive variables in silicic magmas. Contributions to Mineralogy and Petrology 108, 485–510.

Grigsby, J. D. 1990. Detrital magnetite as a provenance indicator. Journal of Sedimentary Research 60(6), 940-95.

Hakyemez, Y. H., Papak, İ. 2002. 1:500000 Scale Geological Inventory Map Series of Turkey, Samsun sheet, General Directorate of Mineral Research and Exploration, Ankara.

Hou, B., Keeling, J., Reid, A. J., Warland, I., Belousova, E., Frakes, L. A., Hocking, R., Fairclough, M. 2011. Heavy mineral sands in the Eucla Basin, southern Australia: deposition and province-scale prospectivity. Economic Geology 106, 687–712.

Hou, B., Keeling, J., Van Gosen, B. S. 2017. Geological and exploration models of beach placer deposits, integrated from case-studies of Southern Australia. Ore Geology Reviews 80, 437-459.

Hutton, C. O. 1950. Studies of heavy detrital minerals. Geological Society of America Bulletin 61, 635-710.

Kadıoğlu, Y. K., Kariper, İ. A., Üstündağ, İ. 2022. Determination of the chemical composition and Raman characterization of barite samples from Denizli and Akdağmadeni, Turkey, using Energy Dispersive X-ray fluorescence and Raman microscopy. Journal of the Indian Chemical Society 99(9), 100659.

Kasper-Zubillaga, J. J., Linares López, C., Espino de la Fuente Muñoz, C. A. 2016. Provenance of opaque minerals in coastal sands, western Gulf of Mexico, Mexico. Boletín de la Sociedad Geológica Mexicana 68(2), 323-338.

Kasper-Zubillaga, J. J., Martínez-Serrano, R. G., Arellano-Torres, E., Alvarez Sanchez, L. F., Patiño Andrade, D., Gonzalez Bermudez, A., Carlos-Delgado, L. 2021. Petrographic and geochemical analyses of dune sands from southeastern Mexico, Oaxaca, Mexico. Geological Journal 56(6), 3012-3034.

Kaymakcı, N., Graham, R., Bellingham, P., Horn, B. W. 2014. Geological Characteristics of Black Sea Basin: Inferences from New Black Sea Seismic Data. AAPG International Conference & Exhibition, 14-17 September 2014., İstanbul.

Köksoy, M. 1973. Magnetite placer deposits of eastern part of Black Sea coast: MTA, 50. (unpublished).

Kuşcu, İ. 2019. Skarns and Skarn Deposits of Turkey. Pirajno F. (Ed). Mineral resources of Turkey. Modern Approaches in Solid Earth Sciences, 16, 283-336.

La Tour, T. E. 1989. Analysis of rocks using X-ray fluorescence spectrometry. The Rigaku Journal 6(1), 3-9.

Li, C., Yang, S. 2010. Is chemical index of alteration (CIA) a reliable proxy for chemical weathering in global drainage basins? American Journal of Science 310(2), 111-127.

Lohmeier, S., Lottermoser, B.G., Strauß, K., Adolffs, T., Sindern, S., Gallhofer, D. 2021. Nearshore marine garnet and magnetite placers in the Erongo and S-Kunene regions, Namibia. Journal of African Earth Sciences 180, 104221.

McDonough, W. F., Sun, S. S. 1995. The composition of the Earth. Chemical Geology 120(3-4), 223-253.

McLennan, S. M., Taylor, S. R. 1991. Sedimentary rocks and crustal evolution: Tectonic setting and secular trends. The Journal of Geology 99, 1–21.

McLennan, S. M., Taylor, S. R., Ericksson, K. A. 1983. Geochemistry of Archaean Shales from the Pilbara Supergroup, Western Australia. Geochimica et Cosmochimica Acta 47, 1211-1222.

McLennan, S.M., Taylor, S.R., McCulloch, M.T., Maynard, J.B. 1990. Geochemical and Nd-Sr isotopic composition of deep sea turbidites: Crustal evolution and plate tectonic associations. Geochimica et Cosmochimica Acta 54, 2015-2050.

McLennan, S. M., Hemming, S., McDaniel, D. K., Hanson, G. N. 1993. Geochemical approaches to sedimentation. Provenance, and tectonics. Special Papers-Geological Society of America, 21-21.

Mollo, S., Putirka, K., Iezzi, G., Scarlato, P. 2013. The control of cooling rate on titanomagnetite composition: Implications for a geospeedometry model applicable to alkaline rocks from Mt. Etna volcano. Contributions to Mineralogy and Petrology 165, 457-475.

Morton, A. C. 1991. Geochemical studies of detrital heavy minerals and their application to provenance research. Geological Society, London, Special Publications 57(1), 31-45.

Morton, A. C., Hallsworth, C. 1994. Identifying provenance-specific features of detrital heavy mineral assemblages in sandstones. Sedimentary Geology 90(3-4), 241-256.

MTA 1993. Gold and silver inventory of Turkey. Maden Tetkik ve Arama, publication no: 198, 46.

Nadoll, P., Mauk, J. L., Hayes, T. S., Koenig, A. E., Box, S. E. 2012. Geochemistry of magnetite from hydrothermal ore deposits and host rocks of the Mesoproterozoic Belt Supergroup, United States. Economic Geology 107, 1275-1292.

Nagata, T. 1961. Rock magnetism (2nd edition). Maruzen Company, Tokyo, 350.

Nesbitt, H. W., Young, G. M. 1982. Early Proterozoic climates and plate motions inferred from major element chemistry of luties. Nature 299, 715-717.

Nesbitt, H. W., Young, G. M. 1984. Prediction of some weathering trends of plutonic and volcanic rocks based on thermodynamic and kinetic consideration. Geochimica et Cosmochimica Acta 48, 1523–1534.

Nesbitt, H. W., Markovics, G. 1997. Weathering of granodioritic crust, long-term storage of elements in weathering profiles, and petrogenesis of siliciclastic sediments. Geochimica et Cosmochimica Acta 61(8), 1653-1670.

Okay, A. I., Altiner, D., Sunal, G., Aygül, M., Akdoğan, R., Altiner, S., Simmons, M. 2018. Geological evolution of the Central Pontides. Geological Society, London, Special Publications 464(1), 33-67.

O'Reilly, W. 1984. Rock and mineral magnetism. Blackie, Glasgow and London: Chapmann and Hall, New York, 220.

Papadopoulos, A. 2018. Geochemistry and REE content of beach sands along the Atticocycladic coastal zone, Greece. Geosciences Journal 22, 955-973.

Pettijohn, F. J., Potter, P. E., Siever, R. 1987. Petrography of Common Sands and Sandstones. In: Sand and Sandstone. Springer, New York, 139-213.

Pohl, W. 2005. Economic Geology: Principles and Practice. Wiley- Blackwell, Chichester, 663.

Qiu, J., Lu, X. J., Chen, P., Hu, S. G., Wang, G. F. 2011. The SEM and EDS Energy Spectrum Analysis of a Beach Placer. Advanced Materials Research 158, 273-280.

Razjigaeva, N. G., Naumova, V. V. 1992. Trace element composition of detrital magnetite from coastal sediments of northwestern Japan Sea for provenance study. Journal of Sedimentary Research 62, 802–809.

Roy, P. S. 1984. New South Wales estuaries: their origin and evolution. Thom, B.G. (Ed.). Coastal geomorphology in Australia. Academic Press. Sydney, 99–121.

Roy, P. S. 1999. Heavy mineral beach placers in southeastern Australia; their nature and genesis. Economic Geology 94(4), 567-588.

Rudnick, R. L., Gao, S. 2003. The Composition of the Continental Crust. Holland, H.D., Turekian, K.K. (Ed.) Treatise on Geochemistry. Elsevier-Pergamon, 3, 1-64.

Spencer, K. J., Lindsley, D. H. 1981. A solution model for coexisting iron-titanium oxides. American Mineralogist 66:1189-1201.

Stephens, W. E., Calder, A. 2004. Analysis of non-organic elements in plant foliage using polarised X-ray fluorescence spectrometry. Analytica Chimica Acta 527(1), 89-96.

Taylor, S. R., McLennan, S. M. 1985. The continental crust: Its composition and evolution. Blackwell., 312.

Van Gosen, B. S., Fey, D. L., Shah, A. K., Verplanck, P. L., Hoefen, T. M. 2014. Deposit model for heavy-mineral sands in coastal environments: U.S. Geological Survey Scientific Investigations Report 2010-5070-L, 51.

Velasco F., Tornos F., Hanchar J. M. 2016. Immiscible iron and silica-rich melts and magnetite geochemistry at the El Laco volcano (northern Chile): Evidence for a magmatic origin for the magnetite deposits. Ore Geology Reviews 79, 346-366.

Yang, S., Wang, Z., Guo, Y., Li, C., Cai, J. 2009. Heavy mineral compositions of the Changjiang (Yangtze River) sediments and their provenance-tracing implication. Journal of Asian Earth Sciences 35(1), 56-65.

Yiğit, 2009. Mineral deposits of Turkey in relation to Tethyan metallogeny: Implications for future mineral exploration. Economic Geology 104(1), 19-51.